Geophysical Journal International

Geophys. J. Int. (2020) **220,** 1149–1171
Advance Access publication 2019 November 11
GJI Geodynamics and Tectonics

doi: 10.1093/gji/ggz508

High-resolution reconstructions and GPS estimates of India–Eurasia and India–Somalia plate motions: 20 Ma to the present

C. DeMets [1], S. Merkouriev[2,3] and S. Jade[4]

[1] *Department of Geoscience, University of Wisconsin-Madison, Madison, WI* 53706, *USA. E-mail: chuck@geology.wisc.edu*
[2] *Pushkov Institute of Terrestrial Magnetism of the Russian Academy of Sciences, Petersburg Filial.* 1 *Mendeleevskaya Liniya, St Petersburg* 199034, *Russia*
[3] *Saint Petersburg State University, Institute of Earth Sciences Universitetskaya nab.*, 7-9, *St. Petersburg* 199034, *Russia*
[4] *CSIR Fourth Paradigm Institute Wind Tunnel Road, Bangalore* - 560037, *India*

Accepted 2019 November 8. Received 2019 November 6; in original form 2019 June 21

SUMMARY

We reconstruct the movement of the India Plate relative to Eurasia at ≈1-Myr intervals from 20 Ma to the present from GPS site velocities and high-resolution sequences of rotations from the India–Somalia–Antarctic–Nubia–North America–Eurasia Plate circuit. The plate circuit rotations, which are all estimated using the same data fitting functions, magnetic reversal sampling points, calibrations for magnetic reversal outward displacement, and noise mitigation methods, include new India–Somalia rotations estimated from numerous Carlsberg and northern Central Indian ridge plate kinematic data and high-resolution rotations from the Southwest Indian Ridge that account for slow motion between the Nubia and Somalia plates. Our new rotations indicate that India–Somalia plate motion slowed down by 25–30 per cent from 19.7 to 12.5–11.1 Ma, but remained steady since at least 9.8 Ma and possibly 12.5 Ma. Our new India–Eurasia rotations predict a relatively simple plate motion history, consisting of NNE-directed interplate convergence since 19 Ma, a ≈50 per cent convergence rate decrease from 19.7 to 12.5–11.1 Ma, and steady or nearly steady plate motion since 12.5–11.1 Ma. Instantaneous convergence rates estimated with our new India–Eurasia GPS angular velocity are 16 per cent slower than our reconstructed plate kinematic convergence rates for times since 2.6 Ma, implying either a rapid, recent slowdown in the convergence rate or larger than expected errors in our geodetic and/or plate kinematic estimates. During an acceleration of seafloor faulting within the wide India–Capricorn oceanic boundary at 8–7.5 Ma, our new rotations indicate that the motions of the India Plate relative to Somalia and Eurasia remained steady. We infer that forces acting on the Capricorn rather than the India Plate were responsible for the accelerated seafloor deformation, in accord with a previous study. India–Eurasia displacements that are predicted with our new, well-constrained rotations are fit poorly by a recently proposed model that attributes the post-60-Ma slowdown in India–Eurasia convergence rates to the steady resistance of a strong lithospheric mantle below Tibet.

Key words: Plate motions; Indian Ocean.

1 INTRODUCTION

The collision of continental India and Eurasia (Fig. 1) during the past 50 Myr has arguably been the most important plate tectonic event of the Cenozoic era. Some long-term and early effects of the collision may have included the Cenozoic drawdown of atmospheric carbon dioxide triggered by the uplift of the Tibetan Plateau (e.g. Raymo & Ruddiman 1992; Garzione 2008), a major reorganization of the Carlsberg and Central Indian Ridges between Chron C18 (39 Ma) and C7 (24 Ma, Mercuriev *et al.* 1995), and the opening of the Red Sea and Gulf of Aden at 29–24 Ma (Bosworth *et al.* 2005; Wolfenden *et al.* 2005). To better understand the timings and causes of these events, numerous authors have reconstructed relative and absolute India Plate motions using seafloor spreading magnetic lineations and fracture zones from an extended plate circuit between the two plates (Fig. 2,Molnar & Tapponnier 1975; Patriat & Achache 1984; Dewey *et al.* 1989; Molnar & Stock 2009; Copley *et al.* 2010; White & Lister 2012; Iaffaldano *et al.* 2013; Gibbons *et al.* 2015) and from palaeomagnetic latitudes estimated from oceanic drill cores (e.g. Klootwijk *et al.* 1992).

Within the past 20 Myr, the period covered by this study, a topic of ongoing interest has been whether widespread faulting and folding of the seafloor south of India, which began at 15.4–13.9 Ma and accelerated sharply at 8.0–7.5 Ma (Gordon *et al.* 1998; DeMets

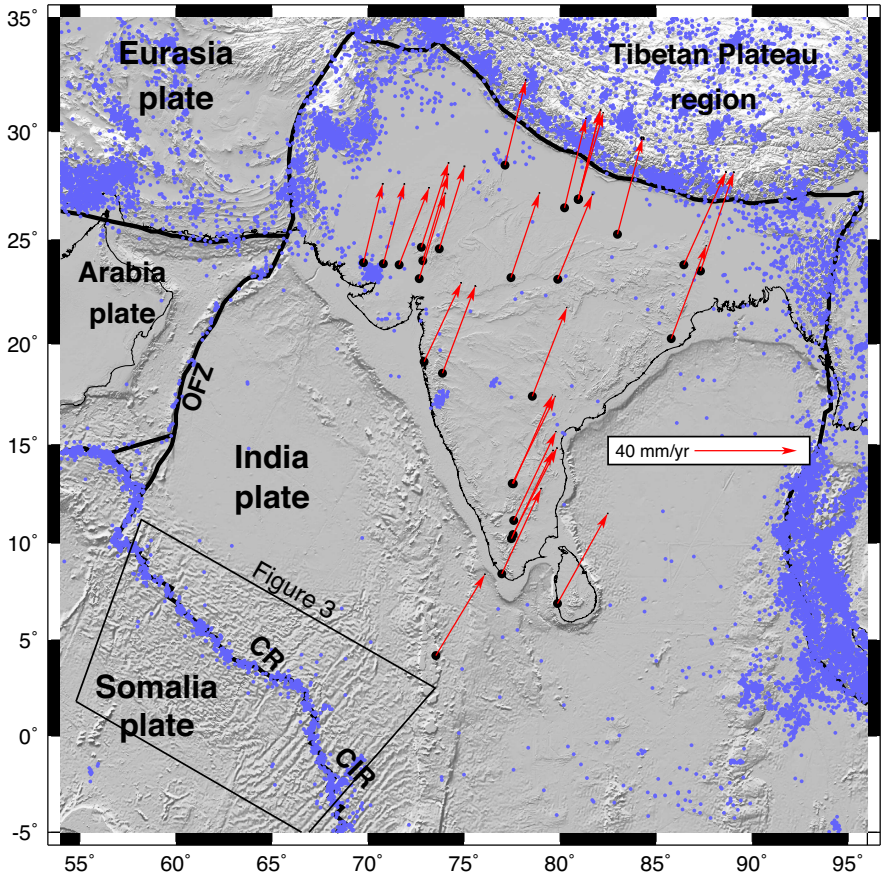

Figure 1. Study area location map with India Plate GPS sites and shallow earthquakes for the period 1964 to late 2016. The red arrows show the velocities of India Plate GPS sites relative to Eurasia that are used in this study to estimate the instantaneous angular velocities for the India Plate relative to the Eurasia and Somalia plates, as described in the text. The boxed area locates the map in Fig. 3, where seafloor spreading data from the Carlsberg Ridge and Central Indian Ridge are used to find closely spaced rotations for magnetic anomalies 1n through 6n. CR, Carlsberg Ridge; CIR, Central Indian Ridge; OFZ, Owen fracture zone.

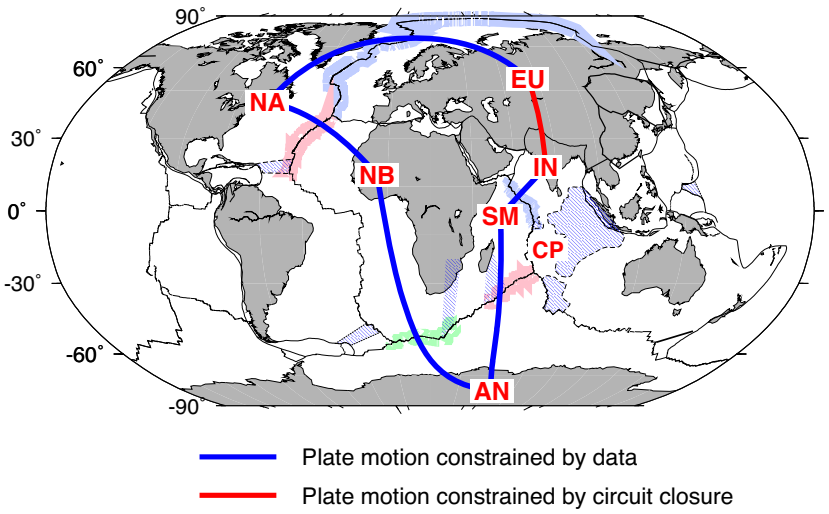

Figure 2. Plate circuit used to estimate India–Eurasia finite rotations and stage angular velocities. The blue-, green- and pink-shaded areas identify the five plate boundaries from which plate kinematic data were used to estimate India–Eurasia plate motion. Plate name abbreviations are as follows: AN, Antarctic; CP, Capricorn; EU, Eurasia; IN, India; NA, North America; NB, Nubia; SM, Somalia.

et al. 2005; Krishna *et al.* 2009; Bull *et al.* 2010), was triggered by the uplift of the Tibetan Plateau, a change in India–Eurasia plate motion (Molnar *et al.* 1993; Harris 2006; Molnar & Stock 2009) or possibly an acceleration of Capricorn plate motion (Iaffaldano *et al.* 2018). Using closely spaced rotations that they derived from plate circuit rotations that connect India to Eurasia (Fig. 2), Molnar & Stock (2009) report evidence for a ≈40 per cent decline in India–Eurasia convergence rates between 20 and ≈10 Ma, with apparently steady rates since at least 10 Ma. Applying similar methods, Iaffaldano *et al.* (2013) also report a significant decline in convergence rates from 20 to ≈10 Ma, but slowly increasing rates since then. Based on evidence for a significant change in Capricorn–Somalia plate motion at 9–5 Ma, but steady India–Somalia plate motion during this period, Iaffaldano *et al.* (2018) propose that the 8–7.5 Ma acceleration of seafloor deformation in the central Indian Ocean basin originated via a change in the forces acting on the Capricorn rather than India Plate, possibly via an increase in the eastward-directed asthenospheric flow associated with the Reunion hotspot plume.

Efforts to test hypotheses about interrelationships between India Plate kinematics and dynamics and important geologic events such as central Indian Ocean seafloor deformation and Tibetan Plateau uplift require estimates of India Plate motion with sufficient accuracy and temporal resolution to detect and quantify changes in plate motion and determine their age to within 1–2 Myr. Reconstructing the movement of India relative to Eurasia from relative motions within the India–Somalia–Antarctic–Nubia–North America–Eurasia plate circuit is challenging because of the cumulative effects of random and possible systematic errors in the lengthy plate circuit. For example, estimates of India–Eurasia rotations in all previous studies lacked reliable reconstructions of slow motion between the Nubia and Somalia plates across the East African rift system. In addition, interpolations between the often widely spaced plate circuit rotations that were combined for all previous estimates of India–Eurasia rotations likely introduced artefacts in the magnitude and timing of their estimated plate motion changes.

In this study, we estimate India–Eurasia plate motion for the first time from high-resolution sequences of rotations for all five plate pairs that connect India to Eurasia, including India–Somalia rotations newly estimated for this analysis, Nubia–Antarctic and Somalia–Antarctic rotations that constrain the slow motion between Nubia and Somalia (Merkouriev & DeMets 2014a; DeMets & Merkouriev 2016), and Nubia–North America and Eurasia–North America rotations not previously used to estimate India–Eurasia motion (Merkouriev & DeMets 2014b; DeMets *et al.* 2015a,b). Along with GPS-based angular velocities that we estimate for the India Plate, we reconstruct India–Eurasia plate motion at 22 distinct times from 19.7 Ma to the present, averaging ≈1-Myr between time steps. Other advantages of this analysis with respect to previous studies include the following: (1) all the best-fitting plate circuit rotations and uncertainties used for our analysis were estimated using the same data fitting functions and methods. (2) All the best-fitting plate circuit rotations were corrected for the biasing effects of magnetic reversal outward displacement. (3) All five plate circuit rotation sequences sample the same 21 magnetic reversals, nearly eliminating the need for any interpolations between rotations, an important source of temporal artefacts in the reconstructed plate motions. (4) Noise-reduced rotation sequences for all five plate circuit pairs are combined in order to mitigate the cumulative impact of random noise on our estimated India–Eurasia rotations.

2 METHODS

2.1 Best-fitting rotations and uncertainties

The methods and fitting functions we use to find India–Somalia rotations that best fit magnetic reversal, transform fault and fracture zone crossings are summarized below and described in detail by Merkouriev & DeMets (2014a). Briefly, all the magnetic reversal, transform fault and fracture zone crossings are inverted simultaneously to find the sequence of finite rotations that minimizes the cumulative weighted least-squares data misfit based on different fitting functions for each type of data. Magnetic reversal crossings are fit using the great-circle fitting criteria of Hellinger (1981); fracture zone crossings are fit using the Shaw & Cande (1990) flow line methodology; transform fault crossings are fit using the small-circle fitting function of Merkouriev & DeMets (2014a). An *a priori* correction is applied to every best-fitting rotation to compensate for outward displacement of the magnetic reversal boundaries, an ubiquitous source of systematic error in finite rotations (DeMets & Wilson 2008). Bootstrap resampling of the spreading segments, fracture zone flow lines, and transform faults that comprise our data is used to estimate covariances for all the best-fitting finite rotations (Merkouriev & DeMets 2014a). The bootstrap resampling algorithm, which samples a wide range of possible data weightings, typically gives rotation uncertainties that are a factor-of-two or larger than the formal covariances (Merkouriev & DeMets 2006).

2.2 Noise-reduced rotations and uncertainties

Sequences of best-fitting rotations that are closely spaced in time sometimes predict erratic, rapid plate velocity changes that may be kinematically and geodynamically implausible (Iaffaldano *et al.* 2014). To reduce this noise, we use REDBACK software, which implements a trans-dimensional, hierarchical Bayesian method to simultaneously mitigate noise in closely spaced best-fitting rotations and quantify the timing and probability of plate motion changes (Iaffaldano *et al.* 2012). The Bayesian algorithm uses a Monte Carlo method to generate millions of candidate finite rotation sequences from an initial sequence of noisy, closely spaced finite rotations and their covariances. Each trial sequence of finite rotations is assigned a probability of being a faithful realization of the true finite rotation sequence based on its distance from the starting rotations. The most representative rotation sequence is defined as the weighted average of the candidate estimates. Nominal covariances are estimated based on the range of candidate models that satisfy the algorithm's acceptability criteria.

2.3 Combining plate circuit rotations and uncertainties

We use standard methods for combining finite rotations for two or more pairs of plates to determine the best-fitting and noise-reduced India–Eurasia finite rotations and their covariances (e.g. Chang *et al.* 1990; Kirkwood *et al.* 1999; Doubrovine & Tarduno 2008). Finite rotations $\hat{A}_{IN\rightarrow EU}$ that reconstruct the India Plate relative to Eurasia were derived following:

$$\hat{A}_{IN\rightarrow EU} = (\hat{A}_{NA\rightarrow EU})(\hat{A}_{NB\rightarrow NA})(\hat{A}_{AN\rightarrow NB}) \times (\hat{A}_{SM\rightarrow AN})(\hat{A}_{IN\rightarrow SM}), \quad (1)$$

where for example $\hat{A}_{IN\rightarrow SM}$ describes the estimated rotation $\hat{A}$ for the India onto the Somalia Plate (see eq. 2 of Doubrovine & Tarduno 2008). The 3x3 covariance matrices $C_{IN\rightarrow EU}$ that describe

the uncertainties in $\hat{A}_{IN\rightarrow EU}$ were determined by propagating the rotation covariances for each of the circuit plate pairs around the plate circuit following eq. (3) from Doubrovine & Tarduno (2008).

In particular,

$$\begin{aligned} C_{IN\rightarrow EU} = &(\hat{A}_{IN\rightarrow NA})^T C_{NA\rightarrow EU} (\hat{A}_{IN\rightarrow NA}) \\ &+(\hat{A}_{IN\rightarrow NB})^T C_{NB\rightarrow NA} (\hat{A}_{IN\rightarrow NB}) \\ &+(\hat{A}_{IN\rightarrow AN})^T C_{AN\rightarrow NB} (\hat{A}_{IN\rightarrow AN}) \\ &+(\hat{A}_{IN\rightarrow SM})^T C_{SM\rightarrow AN} (\hat{A}_{IN\rightarrow SM}) \\ &+C_{IN\rightarrow SM}, \end{aligned} \quad (2)$$

where for example $\hat{A}_{IN\rightarrow AN} = \hat{A}_{SM\rightarrow AN}\hat{A}_{IN\rightarrow SM}$. The operations in (2) transform the covariances $C_{NA\rightarrow EU}$, $C_{NB\rightarrow NA}$, $C_{AN\rightarrow NB}$, and $C_{SM\rightarrow AN}$ into the India Plate coordinate system. Operations related to (2) were carried out with the ADDROT algorithm [Royer & Chang 1991, also see eq. (19) in Kirkwood *et al.* 1999].

The bootstrapping method that is used to estimate the covariances for all the best-fitting rotations gives the same covariances no matter which plate is held fixed when estimating a best-fitting rotation (i.e. the bootstrap covariances are invariant to the frame of reference in a two-plate reconstruction). The finite rotation covariances estimated by REDBACK are similarly invariant to the plate that is held stationary in a two-plate reconstruction.

Stage rotations that describe plate motion from time t_2 to t_1 were determined using the standard method, that is given finite rotations $\hat{A}_{t_2}$ and $\hat{A}_{t_1}$ that reconstruct Plate B onto Plate A for times t_2 and t_1, the stage rotation $\hat{A}_{t_2\rightarrow t_1}$ that reconstructs the motion of Plate B relative to Plate A from t_2 to t_1 is given by $\hat{A}_{t_1}\hat{A}_{t_2}^{\ T}$. If the covariances for both finite rotations are expressed in a common frame of reference, the stage rotation covariances equal the sum of the covariances for $\hat{A}_{t_2}$ and $\hat{A}_{t_1}$. The stage rotations and their covariances vary depending on whether they are tied to Plate A or B in the above example and should thus be expressed relative to the same plate, most commonly that of the stationary plate (Plate A in the generic example above). The finite rotation covariances that express uncertainties in the movement of the India Plate when rotated into a Eurasia frame of reference using eq. (2) are by convention tied to the moving India Plate. We therefore transformed those covariances to the Eurasia Plate frame of reference prior to estimating India-relative-to-Eurasia stage rotations and their covariances.

We determined stage angular velocities and covariances from the stage rotations by dividing the stage rotation angles by the stage time span and the stage rotation covariances by the square of the stage time span. All the magnetic reversal ages are adopted from the astronomically tuned GTS12 time scale (Hilgen *et al.* 2012; Ogg 2012).

2.4 Rotation interpolations

All five plate-circuit rotation sequences that we use to determine India–Eurasia rotations reconstruct the same 21 magnetic reversals (Table S1) except for chrons C5D and C5E for the Nubia–Antarctic Plate pair, for which the ship and airplane survey coverage along the western third of the Southwest Indian Ridge were too sparse to yield reliable rotation estimates (DeMets *et al.* 2015b). To overcome this, we interpolated Nubia–Antarctic C5D and C5E rotations from the next youngest and oldest rotations for this plate pair—those for chrons 5Cn.3 (16.72 Ma) and 6ny (18.75 Ma). The interpolations were done using the standard method described by Doubrovine & Tarduno (2008).

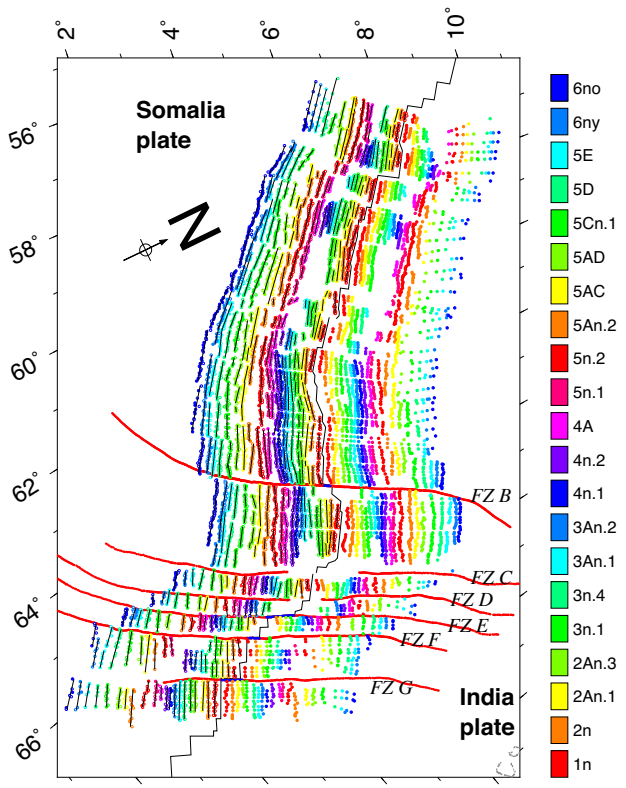

Figure 3. Locations of the 6858 India–Somalia magnetic reversal identifications for Chrons 1n through 6no and reconstructions of India Plate data onto Somalia with their best-fitting rotations from Table 2. The map legend defines the colour that identifies each set of reversal crossings. Fracture zones B–G, which are reconstructed in Fig. 4, are shown by the red circle sequences. The great circle segments that best fit each set of conjugate, reconstructed reversal identifications are shown by the black lines on the Somalia Plate. Reversal identifications that are in their original location are identified with solid symbols (visible upon magnification of the figure). Reversal identifications that have been rotated from their original location on the India Plate to their reconstructed Somalia Plate location are shown by open symbols. The oblique Mercator projection is centred on 35°N, 24.4°W.

3 DATA

3.1 India–Somalia Plate kinematic data

Our new India–Somalia rotations are derived from ≈7000 crossings of 21 magnetic reversals between Chrons C1n and C6no (Fig. 3 and Table S1) and ≈2400 crossings of six fracture zones and four transform faults that offset the Carlsberg and northern Central Indian Ridges (Fig. 3). We use the same magnetic reversal identifications for this study as for our two previous studies of India–Somalia plate motion (Merkouriev & DeMets 2006; Bull *et al.* 2010) with only a few notable differences. First, in order to align our new India–Somalia rotation sequence with the rotation sequences for the other four plate pairs in the global circuit, we identified all crossings of chrons C5AC and C6ny, which were not included in our previous studies, from the shipboard and airborne magnetic data described by Merkouriev & DeMets (2006). Secondly, we revised our interpretations of chron C3n.1 along several Carlsberg Ridge spreading segments. Finally, we added new reversal identifications from several ship tracks that were overlooked in our earlier studies.

The Carlsberg and northern Central Indian ridge fracture zone flow lines and transform faults that constrain our India–Somalia rotations were digitized from Russian ship bathymetry (Merkouriev &

DeMets 2006) and GeoMapApp bathymetry (Carbotte *et al.* 2004, www.marine-geo.org). We digitized the traces of fracture zones B through G (Fig. 3), which are located north of the region where distributed deformation associated with the diffuse India–Capricorn–Somalia triple junction east of the Central Indian Ridge might bias the fracture zone trends (DeMets *et al.* 2005; Drolia & DeMets 2005). We similarly digitized the traces of four well-defined transform faults, all north of or including Fracture Zone G. Individual fracture zone and transform fault crossings were spaced every 1–2 km, the approximate resolution of our bathymetric grid, and were assigned 1σ uncertainties of 0.7–7.5 km based on the quality of the bathymetric mapping and the width and complexity of the fracture zone or transform fault valley.

3.2 Other plate circuit rotations

The best-fitting and noise-reduced rotations for the other four plate pairs that link India to Eurasia were estimated using the same methods as are outlined in Section 2. The best-fitting Eurasia–North America rotations, which were derived from ≈13 200 magnetic reversal, fracture zone, and transform fault crossings from the Arctic basin spreading centres, the Kolbeinsey and Reykjanes Ridges and the Mid-Atlantic Ridge north of the Azores triple junction (Merkouriev & DeMets 2014b), sample all 21 reversals that are listed in Table S1. Via a REDBACK (Bayesian) analysis of these best-fitting rotations, DeMets *et al.* (2015a) derive noise-reduced rotations with misfits to the original magnetic reversal crossings that are only 0–300 m larger than for the best-fitting rotations and less than 1 km larger for the fracture zone flow lines. The noise-mitigated rotations describe a simpler kinematic history than the best-fitting rotations without incurring a significant fitting penalty to the original data.

For the Nubia–North America Plate pair, we use best-fitting and noise-reduced finite rotations from Merkouriev & DeMets (2014b) and DeMets *et al.* (2015a), also for all 21 times listed in Table S1. The best-fitting rotations were estimated from ≈12 900 Mid-Atlantic Ridge magnetic reversal, fracture zone, and transform fault crossings. The fitting penalties for the noise-reduced rotations are a few hundred meters or less for all the reconstructed magnetic reversals and fracture zones, once again too small to be significant (DeMets *et al.* 2015a).

For the Nubia–Antarctic and Somalia–Antarctic Plate pairs, we adopt best-fitting and noise-reduced finite rotations from DeMets *et al.* (2015b). The Nubia-Antarctic rotations for 19 of the 21 times listed in Table S1 were estimated from ∼3500 magnetic reversal, fracture zone, and transform fault crossings from the western third of the Southwest Indian Ridge (0–32°E). The Somalia-Antarctic rotations reconstruct ∼4000 magnetic reversal, fracture zone, and transform fault crossings from the eastern third of the Southwest Indian Ridge (52–70.1°E) at all 21 times in Table S1. The fitting penalties for the noise-reduced rotations for both plate pairs are a few hundred metres or less, too small to be significant (DeMets *et al.* 2015b).

3.3 GPS geodetic data: India, Eurasia and Somalia plates

We estimated instantaneous angular velocities for the India, Somalia and Eurasia plates from the velocities of 97 continuous and 3 campaign GPS sites on the three plates. The data from 78 of the 100 GPS sites are openly available and were processed using GIPSY software (Zumberge *et al.* 1997) and methods described in the Supporting Information. Data from the other 22 sites, all on the India Plate (Jade *et al.* (2017), are proprietary and were processed using GAMIT/GLOBK software (Herring 2003). The data from all 100 stations were processed using orbit and other files appropriate for ITRF2014. The raw GPS observations variously span the period January 1993 to May 2019 (Table S2).

Linear regressions of the weighted daily station Cartesian coordinates were used to estimate individual station velocities and any offsets due to earthquakes or other causes. We did not estimate and correct for transient effects associated with earthquakes, but for several sites, we downweighted or excluded observations from times of obvious transient post-seismic deformation to reduce their effect on the estimated site velocity. We also did not estimate and remove seasonal terms. This had little effect on the velocities of the 71 sites on the Eurasia and Somalia plates, most of which had time-series longer than 10 yr and only one of which had a time-series shorter than 3 yr (Table S2).

Table S2 specifies the velocities of all 100 GPS sites relative to ITRF2014 (Altamimi *et al.* 2016). Displays of the coordinate time-series and text files with the daily east, north and vertical displacements for all 29 India Plate GPS sites are included in the Supporting Information given that the restricted data for 22 of the sites are not otherwise available for inspection.

Fig. 1 shows the velocities of all 29 India Plate GPS sites that were used to estimate the India plate angular velocities relative to ITRF2014 and the Eurasia and Somalia plates (the site codes are shown in Fig. S1 for convenience). The India-ITRF2014 angular velocity that best fits the 29 GPS site velocities (Table 1) has respective weighted root-mean-square (WRMS) misfits of 1.05 and 0.85 mm yr^{-1} to the velocity components that are parallel (tangential) and orthogonal (radial) to small circles about the best-fitting India-ITRF14 pole (Fig. S2). The 13 stations with the best-determined velocities, those with time-series longer than 3 yr, have a cumulative data importance of 2.13, equal to 71 per cent of the information that constrains the three parameters that describe the best-fitting angular velocity. The remaining information (29 per cent) is contributed by the more uncertain velocities for the 16 sites with time-series shorter than 3 yr. The WRMS misfits for the 13 sites with longer time-series are 0.74 and 0.68 mm yr^{-1} for the tangential and radial velocity components, roughly half the 1.70 mm yr^{-1} tangential and 1.24 mm yr^{-1} radial misfits for the 16 sites with shorter time-series.

The residual velocities for the 29 India Plate GPS sites do not reveal any patterns consistent with possible deformation of the plate interior, in accord with conclusions reached by Jade *et al.* (2017). Reduced chi-square, the least-squares misfit to the 29 site velocities normalized by the degrees of freedom, is 2.04. The average weighted misfits are thus ≈40 per cent larger than the estimated velocity uncertainties. We accordingly increased the covariances of the India-ITRF2014 angular velocity listed in Table 1 by a factor of 2.04 relative to the formal covariances to compensate for the underestimated velocity uncertainties.

We estimated the Eurasia-ITRF2014 angular velocity from the velocities of 60 GPS sites well distributed in the plate interior (Fig. S3), taking care to exclude stations from known areas of internal plate deformation such as Fennoscandia, where measurable post-glacial isostatic rebound occurs. The best-fitting angular velocity (Table 1) has respective WRMS misfits of 0.3 and 0.4 mm yr^{-1} to the tangential and radial velocity components. Reduced chi-square is 1.78, indicating that the average weighted misfits are ≈30 per cent larger than the estimated velocity uncertainties. The Eurasia Plate angular velocity covariances in Table 1 were accordingly increased by a factor of 1.78 relative to their formal estimates.

We estimated the Somalia-ITRF14 angular velocity from the velocities of 11 GPS sites selected to avoid areas of distributed deformation along the plate boundaries (Saria *et al.* 2014). The 11 site velocities (see Fig. S4) are well fit by their best-fitting angular velocity (Table 1), with WRMS misfits of 0.6–0.7 mm yr^{-1} to the two velocity components. Reduced chi-square for the best-fitting angular velocity is 1.84, indicating that the average weighted misfits are 36 per cent larger than the estimated velocity uncertainties. The Somalia Plate angular velocity covariances in Table 1 were accordingly increased by a factor of 1.84.

The angular velocities and angular velocity covariances for all three plates relative to ITRF2014 are given in Table 1 along with India–Somalia and India–Eurasia angular velocities that we derived by summing the three angular velocities and their covariances. Later in the analysis, we compare the instantaneous relative motions that are predicted by these angular velocities to their corresponding long-term plate motions.

We tested for possible systematic biases between our GAMIT- and GIPSY-derived India Plate site velocities using a simple procedure. We first inverted the velocities of all 28 GAMIT-processed GPS sites on the India Plate to find their best-fitting angular velocity and associated least-squares misfit. We then solved for the angular velocity that best fits the velocities of six India Plate GPS sites for which we processed the data with GIPSY (five of which overlapped the stations whose data were also processed with GAMIT). We then simultaneously inverted all 34 station velocities to find their combined best fitting angular velocity and misfit. An *F*-ratio test comparison of the least-squares misfit for the latter best-fitting angular velocity to the summed least-squares misfits for the GAMIT- and GIPSY-derived angular velocities indicates that the two differ at only the 60 per cent confidence level for 3 versus 28 degrees of freedom. The GAMIT- and GIPSY-derived site velocities are thus consistent at a high confidence level. The GAMIT- and GIPSY-derived India-ITRF2014 angular velocities predict linear site motions that differ by less than 1 mm yr^{-1} and 1.3° at most locations on the India Plate, too small to affect any of our interpretations and conclusions.

4 RESULTS: INDIA–SOMALIA LONG-TERM AND INSTANTANEOUS MOTIONS

4.1 India–Somalia Plate rotations and data fits

Our new sequence of India–Somalia best-fitting rotations (Table 2) was determined from a simultaneous inversion of 6858 crossings of 21 magnetic reversals, 2293 crossings of six fracture zones and 101 crossings of four transform faults from the Carlsberg and northern Central Indian Ridges (Table S1). The rotation covariances were estimated using the bootstrapping method described in Section 2.1. Noise-reduced rotations and covariances, both determined from a REDBACK analysis of the best-fitting rotations, are given in Table 2. The fits, poles and stage velocities for the best-fitting and noise-reduced rotations are described below.

Fig. 3 shows all 6858 reversal crossings in their original locations and rotated onto the Somalia Plate by the best-fitting rotations in Table 2. The WRMS misfits for the reconstructed reversal crossings average 1.7 km and range from 1.3 to 2.2 km per reversal (Table S1), the same as reported in our earlier study (Merkouriev & DeMets 2006). Reconstructing the same reversal crossings with the noise-reduced rotations in Table 2 gives WRMS misfits close to the misfits for the best-fitting rotations (Table S1); for 17 of the 21 magnetic reversals, the WRMS misfit for the noise-reduced rotation exceeds its corresponding best-fitting rotation misfit by less than 0.5 km, a difference we consider to be insignificant.

Fig. 4 compares all six observed fracture zone flow lines to flow lines reconstructed with the best-fitting and noise-reduced rotations. The traces of all six fracture zone flow lines are slightly sigmoidal, which we show below corresponds to a gradual ≈3° anticlockwise rotation of the plate slip direction since 20 Ma. The WRMS flow line misfits for our best-fitting rotation sequence increase from only 0.4 km for the youngest portions of the flow lines to 5–6 km for the oldest portions (Table S1). The increase in misfit with fracture zone age is due partly to the greater difficulty in locating where palaeoslip occurred within older sections of fracture zone valleys, for which survey coverage is often poorer than for fracture zones closer to the ridge axis. The tendency of some seafloor spreading segments to propagate slowly parallel to the ridge and hence cause fracture zone traces to depart from lines of pure slip also contributes to some of the increase in misfit with fracture zone age.

Fig. S5 compares fracture zone flow lines reconstructed with the best-fitting rotations to flow lines reconstructed with the best-fitting rotations from our earlier study (Merkouriev & DeMets 2006). The new flow lines vary more smoothly and thus describe a simpler plate kinematic history than do the latter flow lines. The improvement is attributable to the flow line fitting criteria we use to derive the new best-fitting rotations (Section 2.1), which is more appropriate for fitting fracture zones than the Hellinger (1981) fitting function we used in our earlier study. The same figure also shows that flow lines reconstructed with the noise-reduced rotations in Table 2 vary more smoothly than do the flow lines reconstructed with the new best-fitting rotations, as expected. Given that the simpler, noise-reduced flow lines do not significantly degrade the WRMS misfit (Table S1), the India–Somalia noise-reduced rotations are our preferred estimates.

Table 1. Angular velocities from GPS site velocities.

Plate	GPS	Lat.	Long.	$\dot{\omega}$				Variances and covariances					
pair	sites	(°N)	(°E)	(° Myr^{-1})	$\dot{\omega}_x$, ○	$\dot{\omega}_y$, ○	$\dot{\omega}_z$, ○	σ_{xx}	σ_{yy}	σ_{zz}	σ_{xy}	σ_{xz}	σ_{yz}
EU-ITRF14	60	54.20	260.05	0.258	−0.0260	−0.1484	0.2088	0.52	0.07	0.71	0.10	0.56	0.11
IN-ITRF14	29	51.51	−4.00	0.509	0.3160	−0.0221	0.3983	2.67	43.17	5.22	9.29	2.96	1.37
SM-ITRF14	11	48.76	265.69	0.314	−0.0156	−0.2067	0.2364	6.70	8.47	1.27	6.82	−1.72	1.27
IN-EU	89	27.47	20.26	0.411	0.3421	0.1263	0.1896	3.19	43.24	5.93	9.39	3.52	1.48
IN-SM	40	23.11	29.10	0.413	0.3316	0.1846	0.1620	9.37	51.64	6.54	16.11	1.24	2.64

These angular velocities describe rotation of the first listed plate relative to either ITRF14 or the second listed plate. The ITRF14 reference frame is constrained to evolve in a manner identical to ITRFTRF14 (Altamimi *et al.* 2016), hence the angular velocities are the same as if ITRFTRF14 were the geodetic reference frame. The columns labelled 'Lat.', 'Lon.', and $\dot{\omega}$ specify the pole coordinates and angular rotation rate of the angular velocity that best fits the GPS station velocities. Angular velocity covariances have units of 10^{-9} radians^2 Myr^{-2}. EU, Eurasia Plate; IN, India Plate; SM,- Somalia Plate.

4.2 India–Somalia poles: best-fitting and noise-reduced

The best-fitting and noise-reduced poles (Table 2) are clustered within a few arc degrees of 23°N, 31°E (Fig. 5), close to the MORVEL 3.16-Myr-average pole (DeMets *et al.* 2010). The poles for reversals older than Chron C5AD (14.61 Ma) are typically several angular degrees farther from the Carlsberg Ridge than are the poles for reversals younger than C5AD, consistent with a modest migration of the pole toward the plate boundary since ≈15 Ma. On average, the new poles are located ≈1–2 angular degrees north of the India–Somalia rotation poles of Merkouriev & DeMets (2006) and Bull *et al.* (2010). We attribute this change to the improved constraints that the fracture zone flow lines impose on the pole locations.

4.3 India–Somalia stage velocities and realistic uncertainties

Fig. 6 shows India–Somalia seafloor spreading rates and directions since 20 Ma near the present geographic centre of the Carlsberg Ridge as estimated with angular velocities variously derived from

Table 2. India–Somalia finite rotations and covariances

Chron	Age	Lat.	Long.	Ω	Covariances					
	(Ma)	(°N)	(°E)	(deg.)	a	b	c	d	e	f
					Best-fitting					
1n	0.781	23.05	31.28	0.306	1.3	2.0	−0.1	5.5	0.2	0.6
2n	1.778	23.96	33.64	0.726	1.2	1.4	−0.4	3.3	0.6	1.1
2An.1	2.581	24.24	31.13	1.008	1.3	1.5	−0.6	4.5	0.7	1.5
2An.3	3.596	21.93	35.54	1.560	2.1	2.0	−1.0	5.1	1.1	2.5
3n.1	4.187	24.30	30.03	1.646	15.9	20.2	−4.6	33.6	−0.1	6.4
3n.4	5.235	22.97	32.83	2.161	3.0	2.8	−1.2	6.3	0.3	1.8
3An.1	6.033	23.40	30.80	2.390	3.0	2.7	−0.8	7.2	0.9	2.4
3An.2	6.733	22.81	31.76	2.699	4.1	2.3	−3.1	5.9	1.2	5.3
4n.1	7.528	22.91	31.77	2.998	3.3	4.0	−1.6	9.6	0.8	3.4
4n.2	8.108	22.74	31.52	3.257	1.8	1.9	−0.9	7.8	1.7	2.4
4A	9.105	23.19	30.96	3.623	2.2	1.0	−2.0	5.9	2.7	4.6
5n.1	9.786	23.60	30.52	3.840	4.7	2.5	−3.3	8.3	2.7	6.3
5n.2	11.056	23.59	30.68	4.361	2.9	1.9	−1.6	5.5	1.6	3.5
5An.2	12.474	24.32	29.73	4.847	4.0	3.2	−2.0	7.8	1.7	4.2
5AC	13.739	23.54	32.02	5.594	12.1	5.1	−9.4	15.8	6.6	17.7
5AD	14.609	25.00	29.46	5.717	10.0	1.7	−11.1	9.6	3.5	16.6
5Cn.1	15.974	25.15	29.79	6.379	10.0	−1.2	−12.0	7.9	6.1	18.5
5D	17.235	25.04	31.01	7.168	23.8	−3.0	−26.6	10.7	10.5	35.7
5E	18.056	25.28	30.90	7.625	21.9	−6.1	−27.5	16.7	17.2	42.4
6ny	18.748	25.34	30.72	7.981	32.1	−1.8	−35.0	22.7	17.0	51.0
6no	19.722	25.49	30.36	8.384	14.6	8.0	−8.5	24.1	4.4	12.3
					Noise-reduced					
1n	0.781	−23.34	212.66	−0.315	16.3	8.8	9.9	6.4	7.8	9.6
2n	1.778	−23.29	212.56	−0.719	25.7	9.8	9.2	9.3	12.0	16.2
2An.1	2.581	−23.23	212.47	−1.044	36.6	10.8	8.4	12.7	16.9	23.7
2An.3	3.596	−23.13	212.32	−1.467	61.9	16.8	12.1	21.0	28.1	39.9
3n.1	4.187	−23.12	212.17	−1.701	67.0	15.1	8.5	22.2	30.3	43.8
3n.4	5.235	−23.13	211.90	−2.117	71.3	11.9	3.1	23.1	32.1	47.4
3An.1	6.033	−23.17	211.69	−2.430	76.6	11.9	2.2	24.8	34.6	51.2
3An.2	6.733	−23.21	211.54	−2.705	84.5	13.2	2.7	27.4	38.1	56.1
4n.1	7.528	−23.29	211.38	−3.018	95.8	15.7	4.5	31.2	43.1	63.0
4n.2	8.108	−23.36	211.28	−3.246	105.6	18.7	7.0	34.5	47.4	68.7
4A	9.105	−23.51	211.13	−3.635	126.0	26.5	14.9	41.6	56.2	80.0
5n.1	9.786	−23.63	211.05	−3.900	143.8	34.1	23.0	47.8	63.8	89.5
5n.2	11.056	−23.85	210.92	−4.397	178.8	50.7	40.9	60.0	78.5	107.5
5An.2	12.474	−24.10	210.80	−4.957	218.1	71.7	64.8	73.7	94.5	126.1
5AC	13.739	−24.32	210.71	−5.487	251.2	89.6	84.9	85.2	107.9	141.9
5AD	14.609	−24.48	210.65	−5.841	251.7	93.8	91.1	85.5	107.5	139.9
5Cn.1	15.974	−24.71	210.57	−6.467	245.9	93.8	92.3	83.4	104.3	135.0
5D	17.235	−24.92	210.50	−7.123	183.6	56.0	48.6	61.7	79.6	106.8
5E	18.056	−25.06	210.46	−7.536	141.7	27.7	15.1	47.0	63.2	89.0
6ny	18.748	−25.18	210.42	−7.874	114.8	5.3	−12.6	37.2	53.0	79.0
6no	19.722	−25.35	210.35	−8.355	94.6	−17.9	−42.3	30.3	46.8	74.9

Note: These finite rotations reconstruct the Somalia Plate onto the India Plate and include an adjustment for 3.5 km of outward displacement. The rotation angles Ω are positive anticlockwise. The rotations and their covariances are determined using methods described in the text. The covariances have units of 10^{-8} radians^2. Elements a, d and f are the variances of the (0°N, 0°E), (0°N, 90°E) and 90°N components of the rotation. The covariance matrices are reconstructed as follows: $\begin{pmatrix} a & b & c \\ b & d & e \\ c & e & f \end{pmatrix}$.

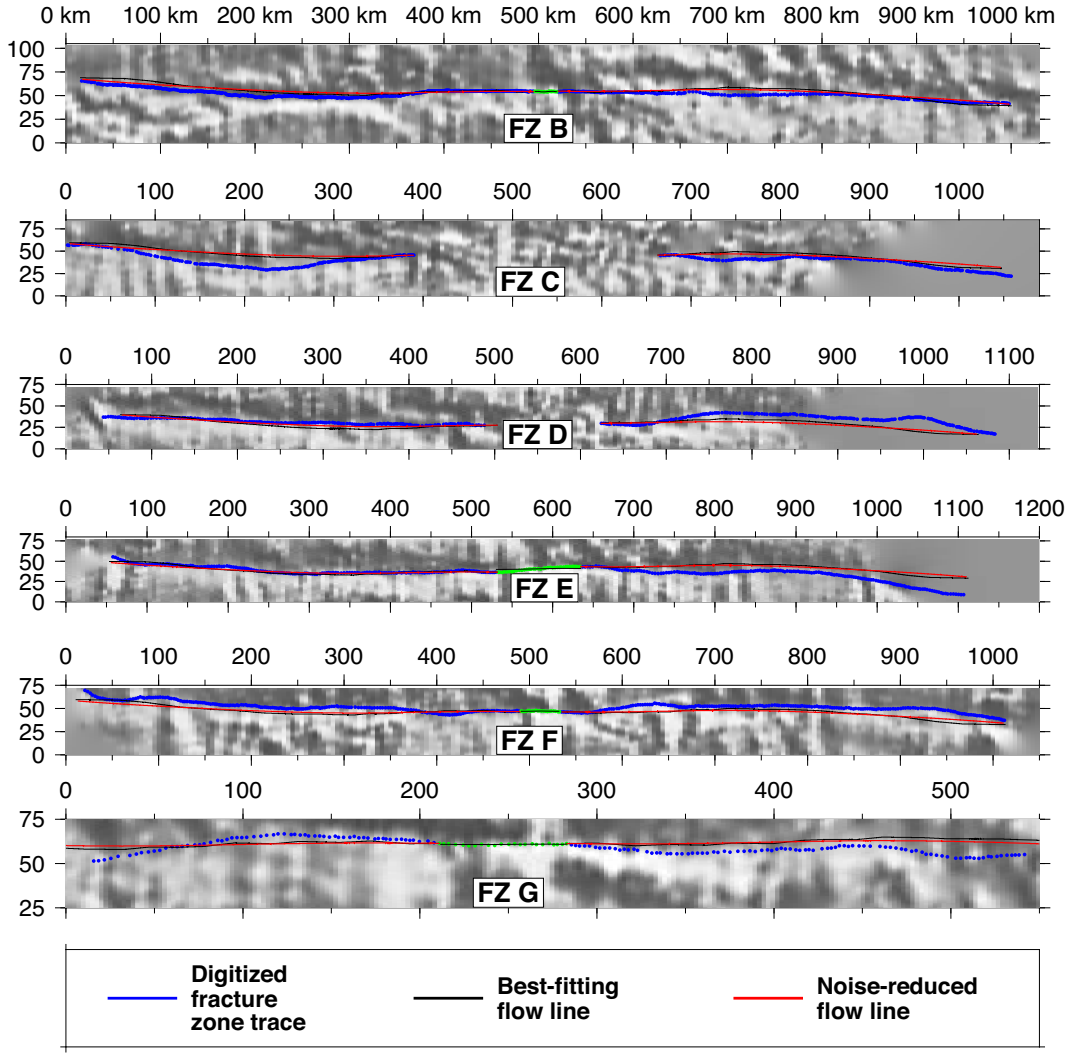

Figure 4. Fits of India–Somalia flow lines estimated with stage rotations derived in this study (red and black lines) to fracture zone flow lines digitized from bathymetry (blue lines). The green circles for fracture zones B, E, F and G show the digitized locations of their transform faults, which constrains the Chron 1n rotation. The best-fitting and noise-reduced flow lines were derived from rotations respectively given in Table 2. All units in the graph are in kilometers.

our noise-reduced rotations (in Table 3), from our best-fitting rotations, and from the best-fitting rotations in table S3 of Bull *et al.* (2010). The estimated spreading rates declined by 25–30 per cent between ≈17 Ma and 12.47–11.06 Ma (Fig. 6a), after which they remained steady or nearly steady to the present. The newly estimated rates are consistent with those reported by Merkouriev & DeMets (2006) and Bull *et al.* (2010), as expected given that many of the same data were used to derive them.

The spreading rates estimated with our best-fitting stage rotations (blue symbols in Fig. 6) exhibit several variations that merit consideration. We interpret five to ten per cent variations in the best-fitting seafloor spreading rates between 9 and 3 Ma (blue circles in Fig. 6a) as likely artefacts of small but systematic misidentifications of the precise locations of one or more magnetic reversals. In particular, the ≈3 mm yr^{-1} difference between the best-fitting rates for the 6.03–4.19 Ma and 4.19–2.58 Ma intervals (C3An.1–C3n.1 and C3n.1–C2An.1, respectively) is most likely caused by a small but systematic mislocation of the young edge of Chron C3n.1. Fig. S6 shows that the shape of Chron C3n.1n becomes increasingly irregular at spreading rates that are slower than 40 mm yr^{-1}. The irregular anomaly shape makes it difficult to identify the precise location of C3n.1 along the Carlsberg Ridge, where spreading rates have averaged 30–40 mm yr^{-1} for the past 10 Myr. A systematic mislocation of only 1.4 km in our identification of the young edge of Chron 3n.1 would be sufficient to explain the entire 2.8 mm yr^{-1} difference between the 6.03–4.19 Ma and 4.19–2.58 Ma stage rates. Similarly, the young edge of Chron 4n.1, which is the other magnetic reversal associated with a sudden 3 mm yr^{-1} change in the sequence of best-fitting spreading rates (Fig. 6a), is difficult to locate precisely at slow spreading rates due to interference from the nearby, short-duration Anomaly 3Br.2n.

Given the general steadiness of the best-fitting stage rates for the past 12.47 Myr, we inverted the magnetic reversal, fracture zone, and transform fault crossings for chrons C1n to C5An.2 (12.47 Ma), totaling 6178 data and including 14 distinct magnetic reversals, to identify the pole and angular rotation rate that best fit the entire ensemble of data. The misfits of the best-fitting pole and angular rotation rate (23.9°N, 30.4°E, 0.391° Myr^{-1}) to the crossings of the 14 reversals in the C1n-to-C5An.2 sequence differ insignificantly from those of the best-fitting rotations, with differences in their

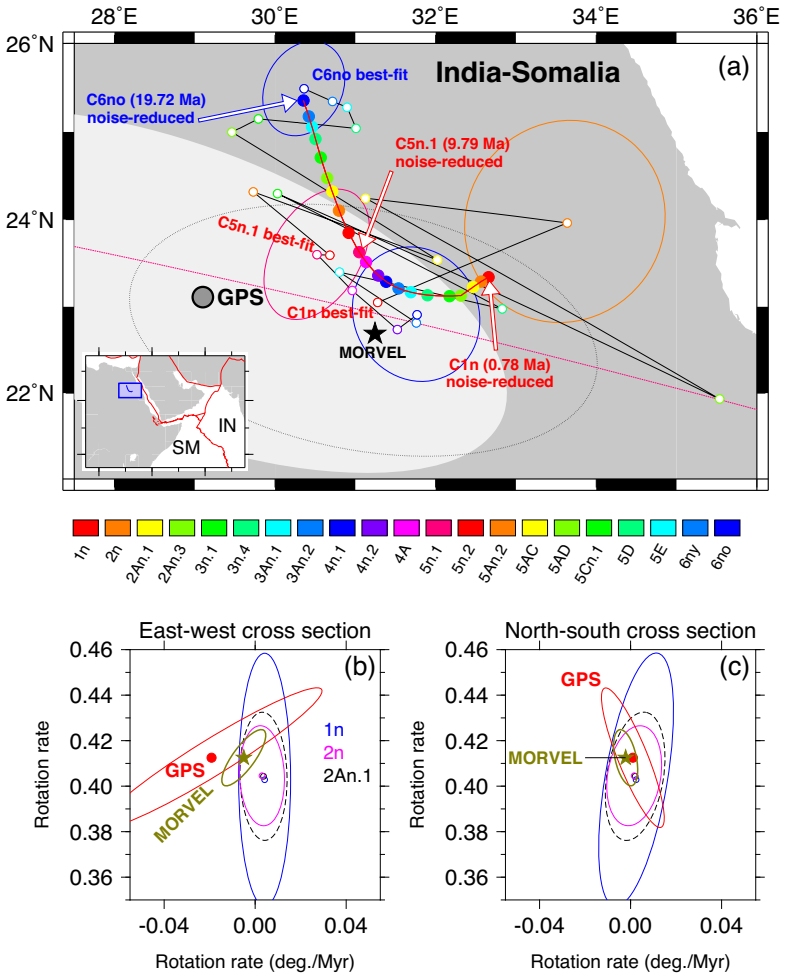

Figure 5. A - Comparison of the India–Somalia GPS pole (Table 1) and best-fitting (open circles) and noise-reduced (solid circles) poles from Table 2. All of the pole confidence ellipses are 2-D 95 per cent. The light shaded region is for the GPS pole. For clarity, other ellipses are shown only for selected magnetic reversals. The blue rectangle in the inset map locates the main map in relation to the regional plate boundaries (red lines). IN; India. SM; Somalia. Panels B and C show projections of the GPS, MORVEL and C1n, C2n and C2An.1 noise-reduced angular velocities onto east–west and north–south vertical cross-sections that pass through 23.0°N, 32.0°E.

respective WRMS misfits that are smaller than 300 m for 11 of the 14 reversals in the sequence and never more than 800 m.

Based on the comparable fits of the constant-motion angular velocity listed in the previous paragraph and the best-fitting rotations in Table 2, we interpret our data as consistent with steady or nearly steady India–Somalia plate motion since 12.47 Ma. The 12.47-Ma-average seafloor spreading rate estimated with the constant-motion angular velocity, 28.6 mm yr^{-1} (grey lines in Fig. 6a), agrees to within ±0.5 mm yr^{-1} with the spreading rates that are estimated with our noise-reduced angular velocities (Table 3) for 13 of the 14 time intervals since 12.47 Ma. That the estimated noise-reduced rates from 12.47 to 9.79 Ma are faster by 0.5–1 mm yr^{-1} than the 12.47-Ma-average spreading rate may indicate that the 25–30 per cent decline prior to 12.47 Ma continued as recently as 9.79 Ma.

The best-fitting and noise-reduced slip directions have remained relatively constant since 20 Ma (Fig. 6b), averaging N35°E near the geographic midpoint of the Carlsberg Ridge and varying by no more than ±2° from the average. The slip directions change more smoothly than the directions estimated with the Bull *et al.* (2010) rotations, which change erratically from one interval to the next (open circles in Fig. 6b). This improvement is directly attributable to the fracture zone flow line fitting function that is used to estimate the best-fitting rotations in this

kii-study.

We interpret the the ±1 mm yr^{-1} scatter of the best-fitting stage rates relative to the noise-reduced rates as an approximation of the realistic 95 per cent uncertainties in our best-fitting stage rates. The 95 per cent uncertainties in the noise-reduced spreading rates, which are derived from the nominal covariances estimated by REDBACK, also average ±1 mm yr^{-1}. We thus consider the spreading rate uncertainties estimated by REDBACK to be realistic for this plate pair.

4.4 Comparison to GPS

Our new GPS-derived India–Somalia rotation pole (Table 1) is located ≈2–3 angular degrees west of the numerous plate kinematic poles (Fig. 5a). The GPS-derived angular velocity (Table 1) predicts an instantaneous spreading rate of 30.6±0.9 mm yr^{-1} (95 per cent uncertainty), 2 mm yr^{-1} faster than estimated with our noise-reduced stage angular velocities (Fig. 6a). Fig. 7(a) emphasizes that

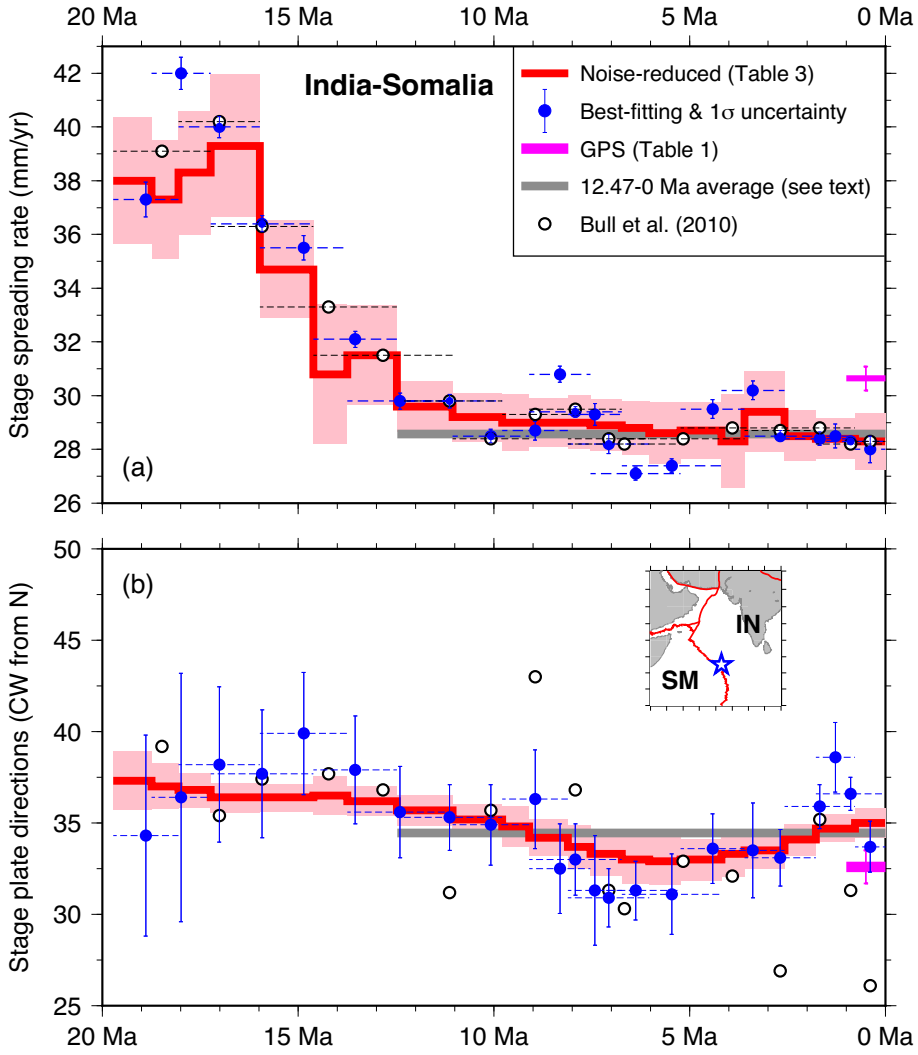

Figure 6. India relative to Somalia forward stage velocities estimated from noise-reduced stage angular velocities in Table 3, best-fitting angular velocities derived from finite rotations in Table 2, and the GPS angular velocity in Table 1. The velocities are estimated along a flow line that originates at 2.6°N, 66.8°E along the Carlsberg Ridge (star in the inset map). (a) Stage spreading rates. The pink shaded region and GPS error bar show the nominal 1σ uncertainties in the noise-reduced and GPS opening rates as propagated from the covariances in Tables 1 and 3. (b) Stage plate slip directions. The horizontal dashed lines shown in both panels span the time intervals associated with the stage rotations. All rates are corrected for outward displacement. IN, India; SM, Somalia.

the instantaneous rates measured at GPS sites on the India Plate (Fig. 7a) are 2–2.5 mm yr^{-1} faster (in a Somalia Plate frame of reference) than the rates predicted with the noise-reduced angular velocities for all intervals since 2.58 Ma. The directions predicted with the noise-reduced angular velocities agree to within 3° (Fig. 6b) or less than 0.5 mm yr^{-1} equivalent (Fig. 7b) with the instantaneous directions indicated by GPS.

We tested the consistency between our new GPS and plate kinematic angular velocities by using the GPS-derived angular velocity to reconstruct the numerous plate kinematic data for Chrons 1n, 2n, 2An.1 and 2An.3. The least-squares misfit for the GPS angular velocity to the numerous data for these four reversals, $\chi^2 = 7891$, greatly exceeds the summed least-squares misfits $\chi^2 = 1468$ for the rotations that best fit the same data. The GPS angular velocity is thus inconsistent with the plate kinematic data.

Interpreted literally, our new GPS angular velocity predicts that Carlsberg and northern Central Indian Ridge seafloor spreading rates have accelerated ≈10 per cent during the past few hundred thousand years. We consider this unlikely given the apparent steadiness of India–Somalia plate motion since at least 10 Ma (see previous section). In Section 6.3, we explore other possible sources of this difference.

5 RESULTS: INDIA–EURASIA LONG-TERM AND INSTANTANEOUS MOTIONS

Table 4 lists the India–Eurasia best-fitting and noise-reduced finite rotations and uncertainties that we derived by applying (1) and (2) to the plate circuit rotations described above. Table 5 lists India–Eurasia angular velocities and covariances we determined from the noise-reduced finite rotations in Table 4. The noise-reduced finite rotations and angular velocities predict a simpler kinematic history for the India–Eurasia Plate pair than do the best-fitting rotations and are thus preferred. For comparisons to the noise-reduced results, we

Table 3. India–Somalia noise-reduced stage angular velocities.

Age	Age	Lat.	Long.	$\dot{\omega}$	Covariances					
(Ma)	(Ma)	(°N)	(°E)	(degrees)	a	b	c	d	e	f
0.000	0.781	23.34	32.66	0.405	15.89	8.57	7.28	7.85	4.86	4.86
0.781	1.778	23.25	32.49	0.406	7.82	3.40	3.17	4.49	2.22	2.61
1.778	2.581	23.09	32.25	0.405	11.65	5.15	4.84	6.72	3.20	3.82
2.581	3.596	22.90	31.94	0.417	30.58	16.17	14.10	15.09	8.65	9.25
3.596	4.187	23.08	31.28	0.396	43.15	22.47	19.52	21.38	12.51	12.80
4.187	5.235	23.19	30.77	0.397	14.43	5.29	5.31	8.70	3.95	4.91
5.235	6.033	23.43	30.29	0.392	16.27	4.96	5.62	10.48	4.28	5.61
6.033	6.733	23.62	30.19	0.394	12.09	2.54	3.44	8.60	2.97	4.84
6.733	7.528	23.97	30.07	0.393	10.41	2.10	3.04	7.54	2.51	4.19
7.528	8.108	24.34	29.98	0.393	12.04	2.78	3.93	8.57	2.85	4.57
8.108	9.105	24.82	29.91	0.391	9.81	2.83	3.62	6.74	2.19	3.71
9.105	9.786	25.24	29.92	0.390	13.87	5.14	5.56	8.47	3.12	5.38
9.786	11.056	25.61	29.95	0.392	9.71	3.85	4.00	5.58	2.36	3.71
11.056	12.474	26.12	29.93	0.395	11.29	5.10	4.97	5.90	2.79	4.29
12.474	13.739	26.39	30.02	0.419	46.90	25.65	23.66	19.63	13.35	14.28
13.739	14.609	26.91	29.78	0.407	88.86	48.85	45.69	36.92	24.87	27.26
14.609	15.974	26.91	29.94	0.459	42.71	23.38	21.67	17.09	12.81	13.15
15.974	17.235	27.03	30.00	0.520	93.88	52.29	48.77	36.55	28.36	28.37
17.235	18.056	27.48	29.86	0.504	69.00	36.51	35.10	29.07	20.15	22.18
18.056	18.748	27.85	29.73	0.489	59.96	28.78	29.07	28.53	15.95	21.94
18.748	19.722	28.34	29.47	0.495	63.91	27.12	29.18	35.68	14.17	27.14

These angular velocities specify India Plate motion relative to the Somalia Plate during the time period given in the first two columns, as determined from the REDBACK noise-reduction software (Iaffaldano *et al.* 2014). They include corrections for 3.5 km of outward displacement, as described in the text. The angular rotation rates $\dot{\omega}$ are positive anti-clockwise. The Cartesian angular velocity covariances, which are defined in the Table 2 caption, are calculated in a Somalia-fixed reference frame and have units of 10^{-8} radians^2 Myr^{-2}. Noise-reduced stage angular velocities and covariances for the Somalia Plate relative to India Plate differ insignificantly from these and are not listed.

also determined but did not tabulate angular velocities from the best-fitting finite rotations.

The best-fitting and noise-reduced poles are clustered near 28°N, 22°E (Fig. 8), several angular degrees from the 3.16-Myr-average MORVEL pole (DeMets *et al.* 2010), but consistent with the new GPS pole (Table 1). The consistency of all the pole locations for times back to 12.47 Ma (C5An.2) suggests that the India–Eurasia pole has been stationary since 12.47 Ma.

5.1 India–Eurasia displacements and stage velocities

Fig. 9 shows the post-19.7-Ma paths of four representative points along the India Plate's northern boundary reconstructed with the noise-reduced India–Eurasia rotations. For times back to and including 12.47 Ma (C5An.2), the reconstructed flow lines differ insignificantly from small circles that are centred on the C5An.2 noise-reduced pole (dashed lines in Fig. 9). The flow lines are thus consistent with a stationary pole location since 12.47 Ma. For times before 12.47 Ma, the reconstructed flow lines are located systematically 10–15 km west of the same small circle paths, consistent with a plate motion change at 12.5 Ma. The reconstructed distances along the 82°E flow line (inset to Fig. 9) are best fit by slopes of 55.3±2.6 km Myr^{-1} (2σ uncertainty) for times before 12.47 Ma and 40.5±0.5 km Myr^{-1} for times since 12.47 Ma, also consistent with a change in plate motion at 12.5±1 Ma.

Convergence rates that we estimated using the noise-reduced and best-fitting angular velocities further reinforce our evidence for a change in India–Eurasia plate motion between 12.47 and 11.06 Ma (Fig. 10). The plate convergence rate declined by ≈50 per cent from more than 60 mm yr^{-1} at 19 Ma to 40 mm yr^{-1} at 12.47 Ma (Fig. 10a), since which the rate has been steady or increased 2–3 mm yr^{-1}. The direction of convergence rotated ≈5° anticlockwise at 12.47 Ma (Fig. 10b), since which it has not varied by more than 1–2°. Within the uncertainties, neither the rotation pole nor the angular rotation rate has changed significantly since at least 11.06 Ma and possibly 12.47 Ma.

5.2 India–Eurasia comparison to GPS

At a central location on the India–Eurasia Plate boundary, our new India–Eurasia GPS angular velocity predicts a convergence direction that is nearly identical to our new plate kinematic estimates (Fig. 10b), but a convergence rate that is 5 mm yr^{-1} slower (Fig. 10a). Given that the GPS and plate kinematic poles are nearly equidistant from the plate boundary (Fig. 11a), the slower convergence rate that is predicted by the GPS angular velocity stems from an angular rotation rate that is 16 per cent slower than our plate kinematic estimates (Figs 11b and c). Fig. 12 highlights the difficulty in reconciling the 4–5 mm yr^{-1} difference between the plate kinematic and GPS estimates, which significantly exceeds the random errors in the highly consistent plate kinematic estimates or the 29 India Plate GPS site velocities.

We consider a literal interpretation of the above, namely that India–Eurasia convergence rates began declining rapidly during the past few hundred thousand years or more recently, to be unlikely given the plate kinematic evidence for steady or slowly increasing convergence rates since 12.47 Ma (Fig. 10a). Other possible causes for the difference are discussed in Section 6.3.

6 DISCUSSION

6.1 Comparison to previous India–Eurasia plate motion estimates

Molnar & Stock (2009) estimate India–Eurasia motion since 67.7 Ma from published rotations from the plate circuit shown in Fig. 2 and estimates of Nubia–Somalia plate motion for Chron C2An.2 (3.16 Ma, Horner-Johnson *et al.* 2007) and Chron C5n.2 (11.06

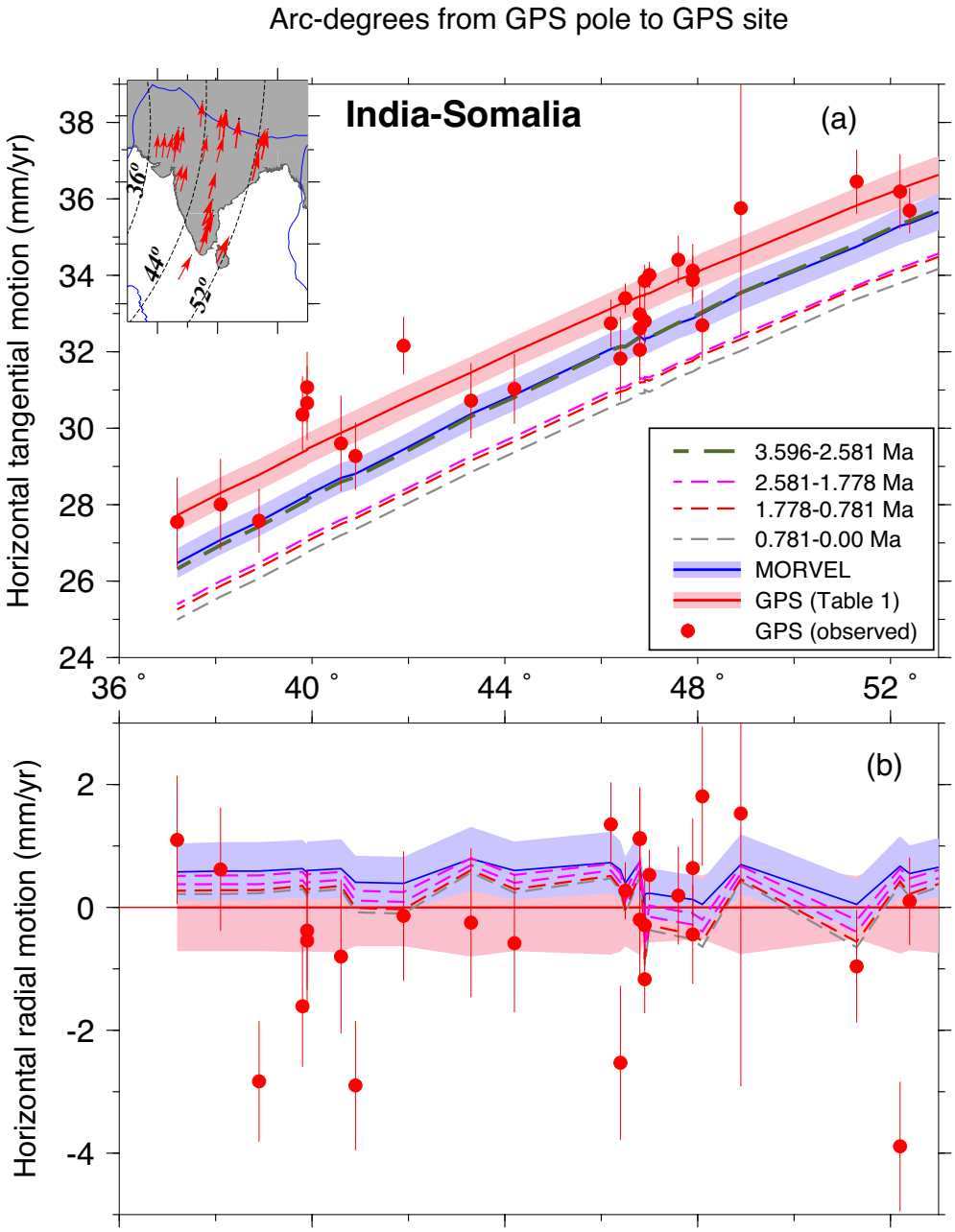

Figure 7. Velocities (filled red circles) of the 29 India (IN) Plate GPS sites transformed to the Somalia Plate frame of reference with the Somalia-IGS14 angular velocity in Table 1. The map inset locates all 29 sites and displays their motions relative to the Somalia Plate. The red lines in (a) and (b) show the velocity components estimated with the India–Somalia GPS angular velocity from Table 1. The dashed lines in (a) and (b) and the legend show India–Somalia velocities estimated with four angular velocities from Table 3 that span the past 3.6 Myr. The velocities estimated with MORVEL (blue lines) average the plate motion over the past 3.16 Myr. The blue and pink shaded regions show 1σ velocity uncertainties. The horizontal axis shows the arc distance from the India–Somalia GPS pole to the 29 India Plate GPS sites (small circles that mark arc distances of 36°, 44° and 52° are shown in the map inset). Panels (a) and (b) show the components of motion that are locally parallel (tangential) and orthogonal (radial) to the small circles in the inset map, which are centred on the best-fitting India–Somalia GPS pole.

Ma, Lemaux *et al.* 2002). Angular velocities determined from their finite rotations predict India–Eurasia convergence rates that decline ≈40 per cent from 20–10 Ma, but remain steady since 10 Ma (blue line in Fig. 13), similar to our results. Our best-fitting and noise-reduced poles are more tightly clustered than their India–Eurasia poles (Fig. 8), as expected given the larger number of data that constrain our plate circuit rotations and the other methods that were used to improve the signal-to-noise ratio in all the rotations. The India–Eurasia flow lines predicted with our rotations are simpler than those predicted with the Molnar & Stock (2009) rotations (Fig. 9), as expected given the tighter clustering of our poles. For times before 11 Ma, the flow lines that are predicted by our respective rotation sequences differ systematically in location by 50–70 km. Roughly two-thirds of this difference is attributable to our improved estimates of Nubia–Somalia plate motion.

Copley *et al.* (2010) use previously published global plate circuit rotations to interpolate India–Eurasia plate motion at 5-Myr intervals since 80 Ma. Convergence rates that are predicted with angular

Table 4. India–Eurasia finite rotations and covariances.

Chron	Age	Lat.	Long.	Ω	Covariances					
	(Ma)	(°N)	(°E)	(°)	a	b	c	d	e	f
					Best-fitting					
1n	0.781	28.30	19.58	−0.377	3.2	1.3	−0.7	6.3	0.1	2.2
2n	1.778	28.63	22.58	−0.858	11.1	7.8	−12.6	13.0	−8.7	27.0
2An.1	2.581	31.27	19.97	−1.211	9.7	5.8	−9.1	12.1	−5.1	23.0
2An.3	3.596	28.97	27.58	−1.772	22.1	10.7	−21.0	15.5	−10.7	43.3
3n.1	4.187	32.39	20.61	−1.980	44.8	34.6	−30.5	52.2	−14.2	63.9
3n.4	5.235	28.55	23.98	−2.562	36.5	16.2	−33.5	24.0	−21.5	69.7
3An.1	6.033	28.21	21.89	−2.829	30.1	11.7	−28.4	24.4	−19.3	63.4
3An.2	6.733	26.21	23.04	−3.160	41.0	16.5	−43.0	29.8	−27.5	85.9
4n.1	7.528	28.80	21.70	−3.507	53.4	29.9	−55.3	46.1	−39.4	94.7
4n.2	8.108	26.23	22.59	−3.796	50.2	21.3	−56.3	38.7	−37.1	105.3
4A	9.105	28.99	20.70	−4.214	78.1	21.3	−73.8	36.6	−39.9	112.5
5n.1	9.786	28.12	23.74	−4.193	101.8	46.5	−96.7	48.6	−58.5	139.3
5n.2	11.056	26.79	21.89	−4.916	31.9	13.0	−31.4	19.2	−17.9	60.5
5An.2	12.474	27.12	21.43	−5.595	38.3	16.9	−37.8	26.9	−24.5	77.8
5AC	13.739	28.07	23.01	−6.531	44.6	18.4	−30.4	41.5	−20.9	82.9
5AD	14.609	29.53	20.93	−6.673	60.1	30.8	−52.1	65.8	−48.9	114.2
5Cn.1	15.974	29.85	20.06	−7.482	229.9	84.3	−246.6	99.5	−150.2	406.6
5D	17.235	29.82	21.35	−8.346	244.2	90.5	−255.2	113.4	−157.8	423.3
5E	18.056	29.82	20.94	−8.812	236.2	87.4	−251.8	112.0	−150.6	438.9
6ny	18.748	29.61	21.39	−9.036	502.8	102.2	−348.1	90.4	−84.0	354.1
6no	19.722	27.23	19.27	−9.990	95.3	47.0	−48.4	88.5	−16.3	103.8
					Noise-reduced					
1n	0.781	28.33	21.87	−0.371	6.4	1.1	1.2	2.7	0.9	4.3
2n	1.778	28.50	22.03	−0.847	9.4	0.9	1.5	4.1	1.2	7.0
2An.1	2.581	28.66	22.19	−1.229	13.0	0.5	2.0	5.7	1.4	10.3
2An.3	3.596	28.67	22.51	−1.719	20.7	0.6	4.0	9.1	2.3	16.9
3n.1	4.187	28.65	22.57	−1.991	23.6	−0.6	4.2	10.6	1.6	20.1
3n.4	5.235	28.39	22.55	−2.474	27.8	−3.1	4.9	13.3	−0.6	25.5
3An.1	6.033	28.15	22.38	−2.836	32.2	−5.0	5.9	16.0	−2.2	30.6
3An.2	6.733	27.99	22.24	−3.152	36.7	−6.2	6.8	18.2	−2.6	35.1
4n.1	7.528	27.91	22.06	−3.508	39.8	−5.9	8.1	19.0	−1.3	37.4
4n.2	8.108	27.84	21.93	−3.766	42.1	−4.7	9.2	19.1	0.5	38.3
4A	9.105	27.85	21.72	−4.202	46.9	−1.2	11.6	19.5	3.7	40.4
5n.1	9.786	27.86	21.62	−4.494	52.6	1.9	14.3	20.7	5.6	43.9
5n.2	11.056	27.71	21.66	−5.051	63.9	7.5	19.7	24.2	7.4	52.6
5An.2	12.474	27.73	21.74	−5.691	77.7	13.6	26.5	29.3	7.4	64.6
5AC	13.739	28.16	21.68	−6.319	96.5	16.7	38.8	35.9	5.8	77.5
5AD	14.609	28.48	21.45	−6.759	105.9	19.0	46.2	34.5	10.1	76.6
5Cn.1	15.974	28.81	20.98	−7.533	113.1	17.3	51.6	31.4	16.4	74.4
5D	17.235	29.03	20.58	−8.327	107.3	9.8	49.5	27.9	17.6	74.2
5E	18.056	29.10	20.21	−8.828	104.0	5.3	49.7	26.8	17.2	76.6
6ny	18.748	28.91	19.97	−9.230	109.2	−0.4	54.8	27.8	14.3	83.4
6no	19.722	28.22	19.97	−9.889	112.4	−20.2	54.1	34.2	−3.1	86.5

Note: These rotations, which reconstruct past positions of the India Plate with respect to the Eurasia Plate, were determined from eq. (1) using best-fitting and noise-reduced rotations described in Sections 3.2 and 4. The rotation angles Ω are positive anticlockwise. The covariances, which have units of 10^{-8} radians^2 and are described in the Table 2 caption, quantify the uncertainties in the reconstructed India Plate positions relative to Eurasia.

velocities we derived from their India–Eurasia finite rotations decrease only 10-15 per cent from 20 Ma to the present, much less than the ≈50 per cent slowdown that is predicted by our rotations (Figs 10 a and 13). The Copley *et al.* rotations predict a 5-Myr-to-present average convergence rate that is 8.5 mm yr^{-1} faster than the GPS-derived convergence rate (Fig. 10a), in even worse agreement than our own new estimates.

Finally, Iaffaldano *et al.* (2013) reconstruct India–Eurasia plate motion since 20 Ma using the same plate circuit as Molnar & Stock (2009), but with more recently published noise-reduced rotation sequences for the Eurasia–North America and India–Somalia plate pairs and exploratory models for Nubia–Somalia plate motion that variously combine Nubia–Somalia finite rotations for chrons C2An.3 (3.16 Ma) and C5n.2 (11.06 Ma) from Lemaux *et al.* (2002), Royer *et al.* (2006), and Horner-Johnson *et al.* (2007). Similar to our results, their models predict that India–Eurasia convergence rates slowed significantly before ≈10 Ma, but remained steady or increased modestly since 10 Ma.

Fig. 13 shows our new India–Eurasia convergence rate estimates in the context of published estimates for the past 45 Ma and several important regional tectonic events. Previous estimates of India–Eurasia plate motion were too noisy and/or sampled the plate motion too infrequently to determine whether significant changes in the plate motion occurred during the 15.4–13.9 Ma onset of

Table 5. India–Eurasia noise-reduced stage angular velocities.

Age	Age	Lat.	Long.	$\dot{\omega}$	Covariances					
(Ma)	(Ma)	(°N)	(°E)	(° Myr^{-1})	a	b	c	d	e	f
	47.090									
0.781	0.00	28.33	21.87	0.474	1.04	0.19	0.20	0.45	0.15	0.70
1.778	0.781	28.62	22.15	0.478	1.59	0.20	0.27	0.69	0.22	1.14
2.581	1.778	29.01	22.55	0.476	3.48	0.20	0.55	1.53	0.41	2.69
3.596	2.581	28.70	23.33	0.483	3.27	0.10	0.59	1.45	0.36	2.64
4.187	3.596	28.51	22.95	0.460	12.64	−0.02	2.39	5.67	1.16	10.57
5.235	4.187	27.34	22.44	0.461	4.66	−0.34	0.84	2.18	0.12	4.16
6.033	5.235	26.47	21.17	0.455	9.36	−1.28	1.71	4.61	−0.39	8.86
6.733	6.033	26.61	20.96	0.451	13.95	−2.30	2.62	6.99	−0.88	13.50
7.528	6.733	27.20	20.49	0.448	12.00	−1.93	2.39	5.91	−0.52	11.53
8.108	7.528	27.05	20.15	0.445	24.15	−3.21	5.23	11.42	−0.04	22.58
9.105	8.108	27.93	19.86	0.437	8.90	−0.62	2.13	3.93	0.49	7.93
9.786	9.105	28.09	20.30	0.430	21.34	0.07	5.65	8.81	2.20	18.16
11.056	9.786	26.51	21.87	0.438	7.19	0.56	2.12	2.82	0.88	5.98
12.474	11.056	27.86	22.36	0.452	7.02	1.03	2.28	2.67	0.83	5.84
13.739	12.474	32.07	21.45	0.498	10.83	1.90	4.05	4.05	0.96	8.97
14.609	13.739	33.10	18.29	0.508	26.57	4.72	11.21	9.30	2.38	20.54
15.974	14.609	31.86	16.94	0.570	11.64	1.94	5.29	3.61	1.52	8.14
17.235	15.974	31.31	16.86	0.631	13.68	1.69	6.45	3.91	2.27	9.35
18.056	17.235	30.42	14.13	0.613	30.79	2.24	14.98	8.66	5.51	22.39
18.748	18.056	25.15	14.70	0.585	43.43	1.16	22.29	12.24	7.13	33.67
19.722	18.748	18.65	19.02	0.687	22.47	−1.97	11.83	6.79	1.38	18.54

Note: Angular velocities that specify India relative to Eurasia Plate motion from the old to the young limits of the time intervals given in the first two columns. The angular rotation rates $\dot{\omega}$ are positive anticlockwise. The angular velocities and Cartesian covariances, which are tied to the Eurasia Plate, are derived from the finite rotations given in Table 6. The covariances, which have units of 10^{-7} radians^2 Myr^{-2}, have been reduced to 20 per cent of their original values so that the stage velocity uncertainties closely approximates the scatter in the stage velocities estimated from the best-fitting rotation sequence. The Table 2 footnotes give further information about the covariances.

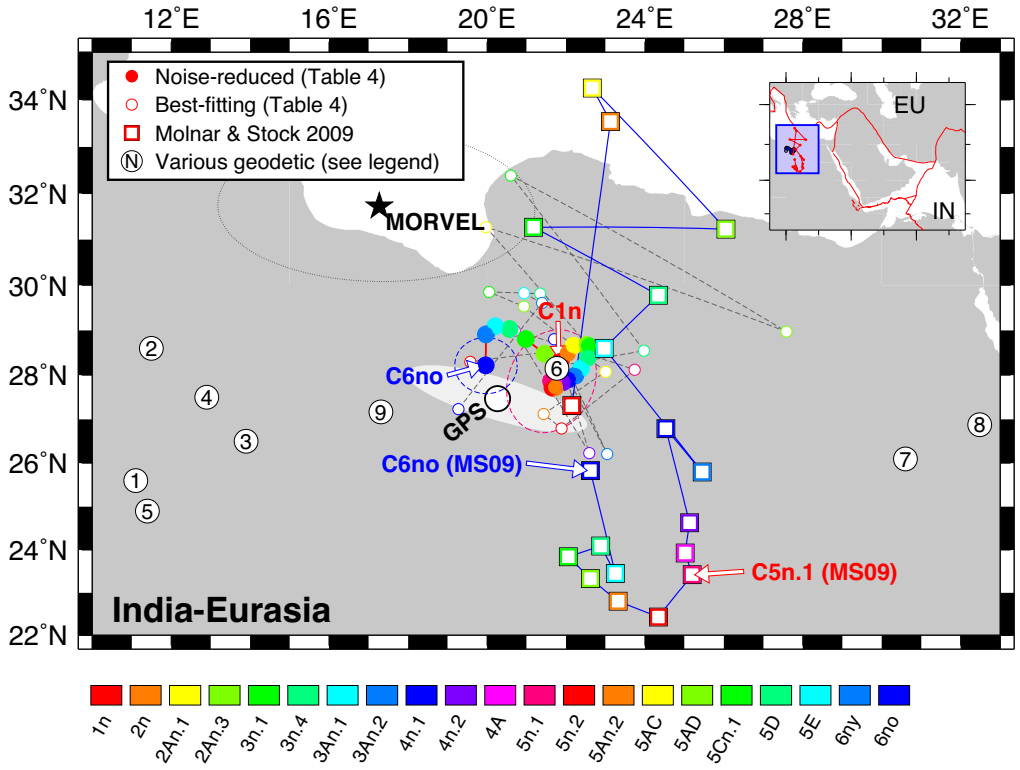

Figure 8. India–Eurasia best-fitting and noise-reduced poles (Table 4) compared to Molnar & Stock's (2009) C1n to C6no India–Eurasia poles (squares). All uncertainty ellipses are 2-D 95 per cent. The blue rectangle in the inset map locates the main map in relation to the regional plate boundaries (red lines). The black symbols in the inset map are the noise-reduced poles from Table 4; the red lines and symbols in the inset map show the Molnar & Stock (2009) poles in the main map. Numbered circles show geodetic poles from 1 - Paul *et al.* (2001), 2 - Sella *et al.* (2002), 3 - Bettinelli *et al.* (2006), 4 - Socquet *et al.* (2006), 5 - Jade *et al.* (2007), 6 - Banerjee *et al.* (2008), 7 - Argus *et al.* (2010), 8 - Altamimi *et al.* (2016) and 9 - Kreemer *et al.* (2014). IN, India; EU, Eurasia.

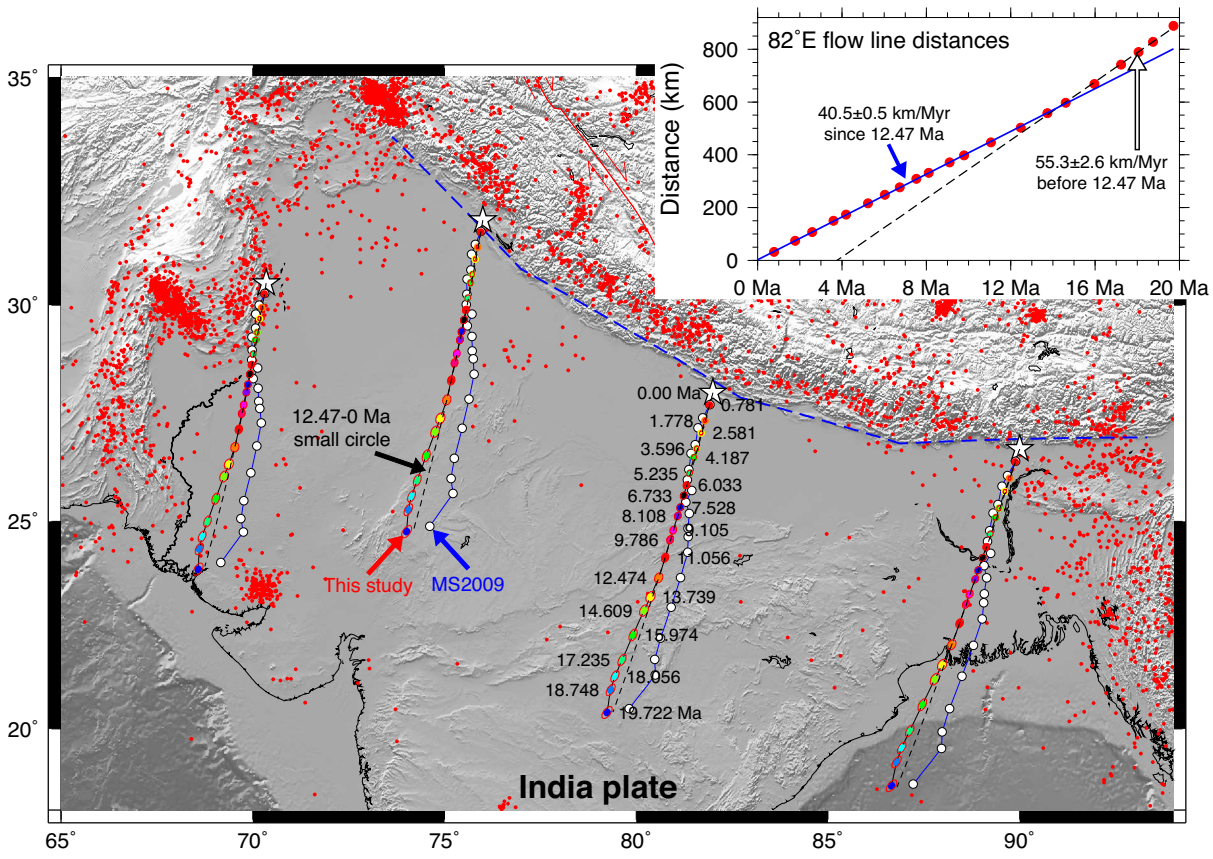

Figure 9. Paths of four India Plate points (open stars) reconstructed with our noise-reduced India–Eurasia rotations (Table 4) and rotations from Molnar & Stock (2009) (abbreviated 'MS2009'). The hard-to-see dashed lines are small circles centred on the noise-reduced pole for C5An.2 from Table 4. Ellipses show the 2-D 95 per cent uncertainties in the reconstructed point locations propagated from the noise-reduced rotation covariances. The labels along one flow line give the ages in Ma of the reconstructed points. The inset shows the cumulative distances for the 82°E flow line predicted with the noise-reduced rotations from Table 4. The 95 per cent uncertainties in the predicted distances, which range from 1.5 to 8 km, are too small to see on the scale of the plot.

distributed seafloor deformation in the central India Ocean or the 8–7.5 Ma deformation speedup (Krishna *et al.* 2009). Our new, better-determined estimates indicate that neither tectonic event coincided with a significant change in the plate motion.

Between 35 and 20 Ma, when major changes occurred in the geometry and kinematics of the Carlsberg Ridge (Patriat & Segoufin 1988; Mercuriev *et al.* 1995) and rifting began across the Gulf of Aden and Red Sea (Bosworth *et al.* 2005; Wolfenden *et al.* 2005), the Molnar & Stock (2009) and Copley *et al.* (2010) plate circuit reconstructions predict India–Eurasia convergence rates that differ by a surprisingly large 50 per cent (Fig. 13). We are presently estimating India plate motion at more closely spaced intervals during this critical period in order to better understand whether and how these events were related to India–Eurasia plate motion.

6.2 Nature of India–Eurasia convergence rate decline since 20 Ma

Clark (2012) shows that 67-Ma-to-present India–Eurasia displacements estimated with rotations from Molnar & Stock (2009) decay exponentially with time, as is predicted by a model in which the rheology of the mantle lithosphere below the Tibetan Plateau and its constant resistance to the plate convergence are assumed to have been the primary factors that control the long-term slowdown in the plate convergence rate. Below, we reconsider the fit of this model based on our new, better constrained India–Eurasia rotations.

Fig. 13 (black line) shows the fit of the best exponential decay model derived by Clark (2012) to convergence rates for the past 20 Ma as estimated with the Molnar & Stock (2009) and our new rotations. Whereas the predicted convergence rates for the Clark (2012) model match the trend that is defined by the noisy rates calculated with former rotations (blue line in Fig. 13), they mismatch our newly estimated convergence rates (compare the red and black lines in Fig. 13). As a test, we inverted our noise-reduced (and best-fitting) displacements $x(t)$ for the India–Eurasia flow line that originates at 28°N, 82°E (displayed in the Fig. 9 inset) using $x(t) = L_o\,(e^{-\dot{\epsilon}t} - 1)$ from Clark (2012) to find best-fitting values for L_o, the width of the India–Eurasia orogenic belt, and $\dot{\epsilon}$, the bulk strain rate in the direction of plate convergence. Reduced chi-squared, the weighted least-squares misfit normalized by the degrees of freedom, is 5.13 for the exponential decay model, indicating that the new displacements are misfit on average by 2.3 times their estimated uncertainties. Sixteen of the 22 displacements are misfit by 1–4 times their estimated uncertainties, emphasizing the poor fit. The fit to the noisier best-fitting displacements is even worse, with reduced chi-square of 12.7 and only two of the 22 displacements fit within their estimated uncertainty.

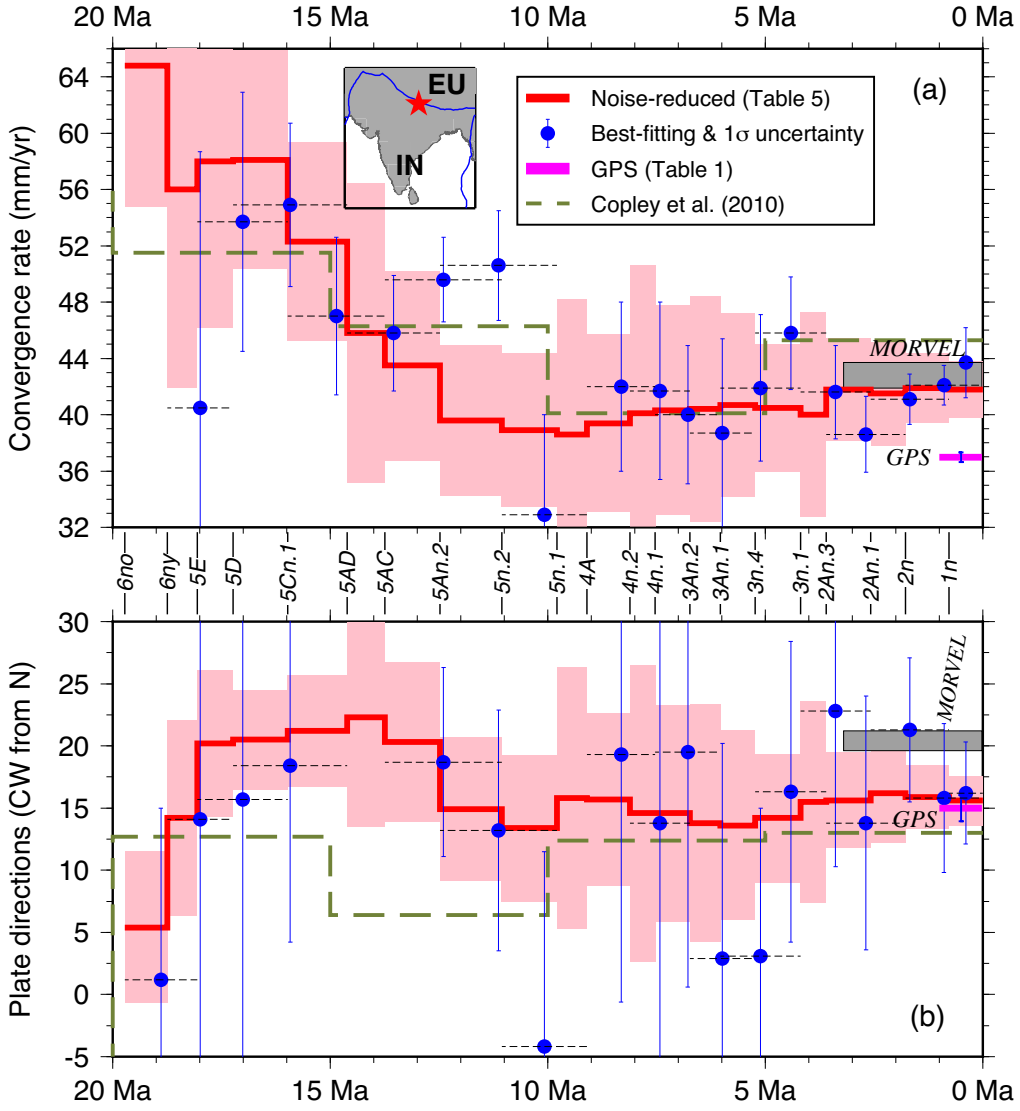

Figure 10. India relative to Eurasia stage rates (a) and directions (b) predicted by noise-reduced angular velocities in Table 5, best-fitting angular velocities (not listed), and the GPS angular velocity in Table 1. Velocities are predicted at 28.0°N, 82.0°E (red star in inset map). Uncertainties indicated by the shaded regions or error bars are 1-σ and are propagated from the angular velocity covariances in Tables 1 or 5. The grey bars show opening rates and directions that are predicted by the MORVEL India–Eurasia 3.16-Myr-average angular velocity (DeMets *et al.* 2010). The purple bar shows the rate and direction predicted by the GPS angular velocity in Table 1.

We also inverted our noise-reduced displacements while fitting them with two slopes and a common distance-axis intercept, which approximates two principal stages of India–Eurasia plate motion since 20 Ma. This alternative model fits the displacements much better, with reduced chi-square of only 1.7 and significant misfits to only 8 of the 22 noise-reduced displacements. The improvement in fit of the two-line model relative to that for the exponential decay model is significant at a probability level better than 99.99 per cent as determined with an F-ratio test for one additional model term.

Our new India–Eurasia rotations are thus fit poorly by a model that enforces exponentially decaying interplate convergence rates during the past 20 Ma. We conclude that the rheology of the mantle beneath Tibet and its resistance to India–Eurasia convergence are unlikely to be the primary factors that determined the plate motion since 20 Ma.

6.3 Implications for central Indian Ocean seafloor deformation

Iaffaldano *et al.* (2018) propose that a change in the forces that were acting on the Capricorn at ≈8 Ma was responsible for an acceleration at 8–7.5 Ma of contractional seafloor deformation in the equatorial Indian Ocean (Krishna *et al.* 2009). From REDBACK analyses of published India–Somalia and Capricorn–Somalia rotation sequences, they report the highest probability for a change in India–Somalia motion just before 15 Ma and Capricorn–Somalia motion just before 5 Ma. Here, we reevaluate when the motions for both plate pairs changed using our new India–Somalia rotations (Table 2) and 20 rotations that describe Capricorn–Somalia plate motion since 19.7 Ma (DeMets *et al.* 2005).

Fig. 13 shows the normalized likelihood of a change in India–Somalia angular rotation rates since 20 Ma as determined from our

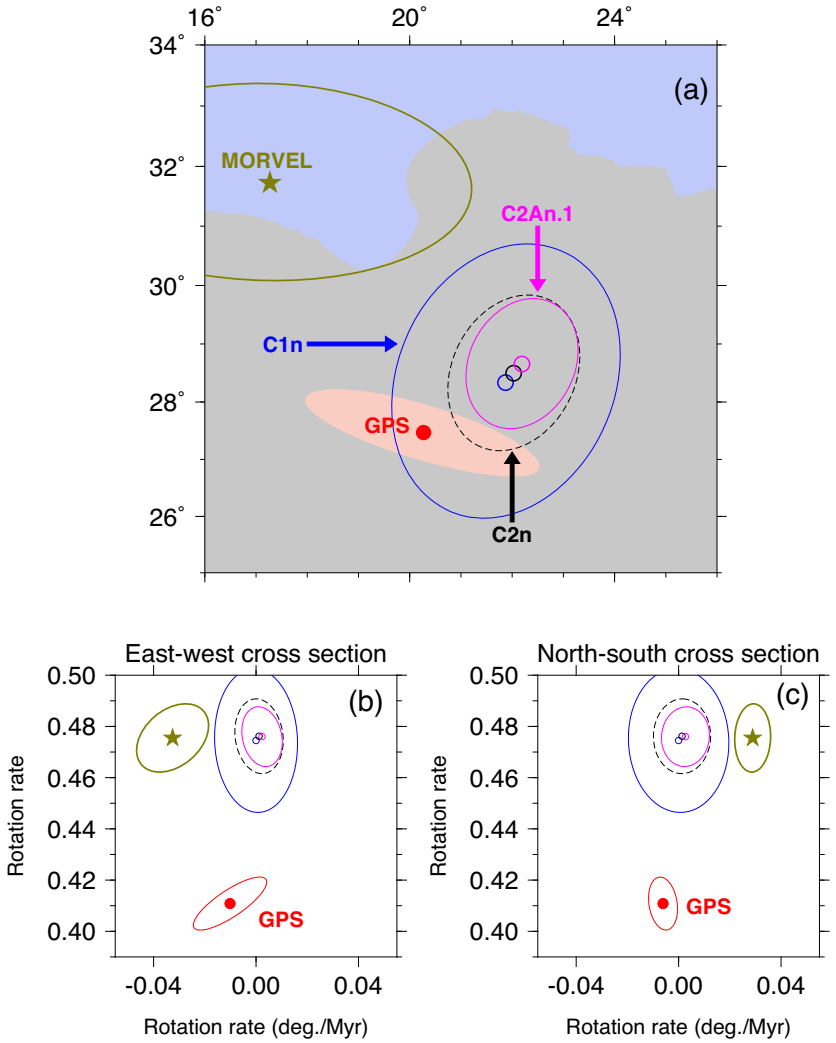

Figure 11. Comparison of India–Eurasia angular velocities and their 2-D 95 per cent confidence regions in three perpendicular planes. Panel (a) shows poles of rotation and 95 per cent confidence ellipses for the GPS angular velocity in Table 1, the MORVEL 3.16-Myr-average angular velocity (DeMets *et al.* 2010), and for Chron 1n, 2n, and 2An.1 noise-reduced angular velocities derived from finite rotations and covariances in Table 4. Panels (b) and (c) show projections of the same angular velocities onto east–west and north–south vertical cross-sections that are centred on the Chron 1n pole (28.3°N, 21.9°E).

REDBACK analysis of the best-fitting India–Somalia rotations in Table 2. The highest probability of a change occurs for the period 17–12.5 Ma, when Carlsberg Ridge seafloor spreading rates were decreasing steadily (Fig. 6a). At a lower probability level, our REDBACK analysis also indicates that the plate motion may have changed at 4–3 Ma. In Section 4.3, we argue that apparent short-duration spreading rate changes between 5 and 3 Ma (Fig. 6a) are artefacts of a 1–1.5-km misidentification of the young edge of Anomaly 3n.1. We conclude that India–Somalia plate motion changed at or before 12.5 Ma, but has remained steady or nearly steady since 12.5 Ma.

Preceding our REDBACK analysis of the Capricorn–Somalia rotations from DeMets *et al.* (2005), we corrected the rotations for an assumed 2 km of outward displacement. Our REDBACK analysis of the corrected rotations reveals a single high-probability change in the Capricorn-Somalia angular rotation rate at 8 Ma (Fig. 13), approximately 3 Myr earlier than the highest probability change reported by Iaffaldano *et al.* (2018) from their analysis of the same sequence of rotations. Our REDBACK analysis thus indicates that the plate motion changed at nearly the same time as the 8–7.5 Ma acceleration of seafloor deformation in the equatorial Indian Ocean.

Any change in Somalia–Capricorn and Somalia–India plate motions that is attributable to a change in the absolute motion of the Somalia Plate should appear in our REDBACK analysis as a high-probability, simultaneous change in the motions for both plate pairs. Our REDBACK analysis instead indicates high-probability changes for the two plate pairs at significantly different times since 20 Ma. We conclude that the ≈8 Ma change in Capricorn–Somalia motion was caused by a net change in the torques acting on the Capricorn Plate, whereas the change in India–Somalia plate motion at or before 12.5 Ma was caused by a net change in the torques acting on the India Plate.

From their analysis of faults imaged in marine seismic transects of the wide oceanic boundary between the Capricorn and India plates, Krishna *et al.* (2009) conclude that seafloor deformation

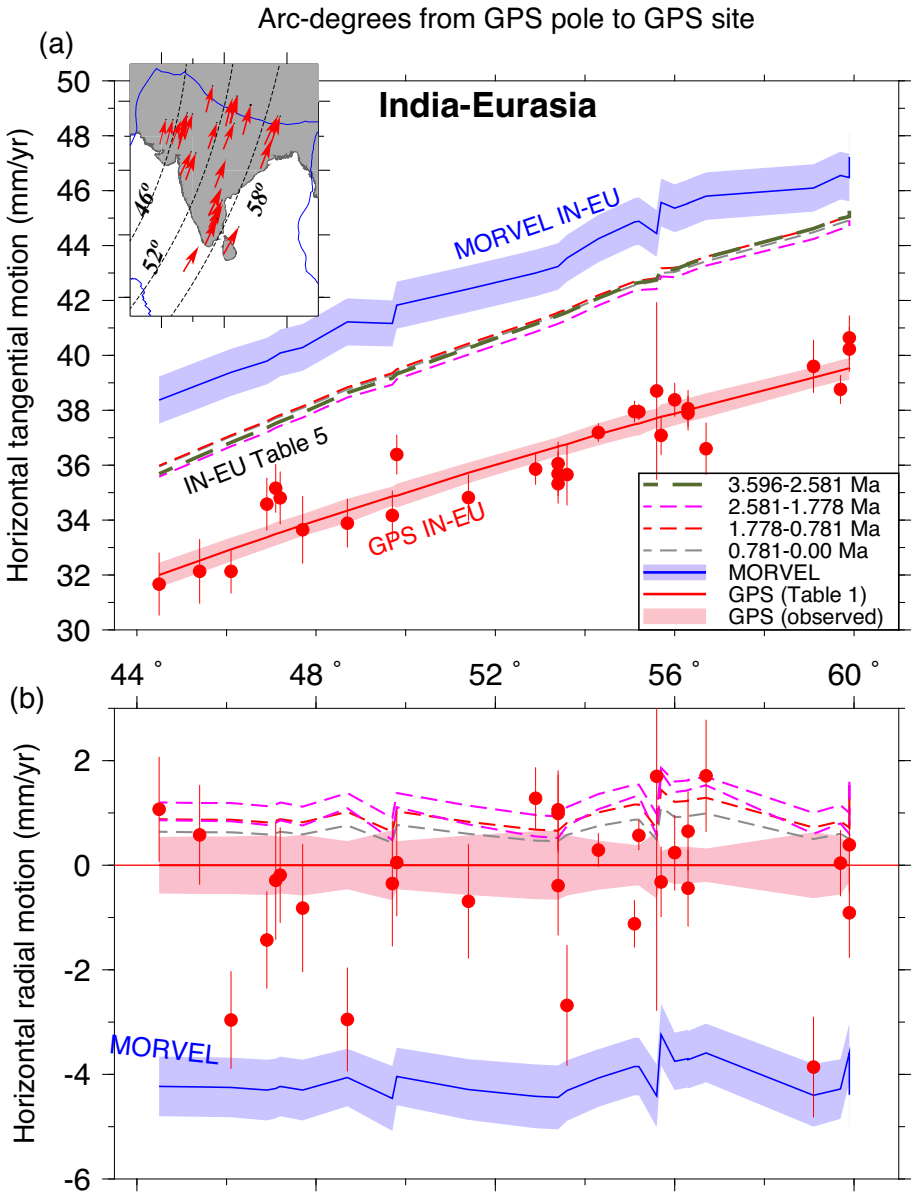

Figure 12. Velocities (filled red circles) of the 29 India (IN) Plate GPS sites transformed to the Eurasia Plate frame of reference with the Eurasia-IGS14 angular velocity from Table 1. The map inset displays the locations of all 29 sites and their motions relative to Eurasia. The red lines in (a) and (b) show the velocity components estimated with the India–Eurasia GPS angular velocity from Table 1. The dashed lines in (a) and (b) and the legend show India–Eurasia velocities estimated with our new stage angular velocities (Table 5). The velocities estimated with MORVEL (blue lines) average the plate motion over the past 3.16 Myr. The blue and pink shaded regions show 1σ velocity uncertainties. The horizontal axis shows the arc distance from the India–Eurasia GPS pole to the 29 India Plate GPS sites (small circles that mark arc distances of 46°, 52° and 58° are shown in the map inset). (a) and (b) show the components of motion that are locally parallel (tangential) and orthogonal (radial) to the small circles in the inset map, which are centred on the best-fitting India–Eurasia GPS pole.

began at 15.4–13.9 Ma and increased sharply at 8–7.5 Ma. The timings of both of these deformation events coincide with the plate motion changes indicated by our REDBACK analyses (Fig. 13). Our analysis supports Iaffaldano *et al.*'s (2018) conclusion that forces acting on the Capricorn plate were responsible for the acceleration of seafloor deformation at 8–7.5 Ma, but indicates even better agreement between the timing of the two events (Fig. 14) than was found in the earlier study.

6.4 Reconciling instantaneous and long-term estimates of India relative plate motions

6.4.1 India–Somalia

Our new GPS angular velocity for India–Somalia plate motion (Table 1) predicts instantaneous motion that is 2–2.5 mm yr^{-1} faster than our plate kinematic estimates (Figs 6 and 7). We consider a 2–2.5 mm yr^{-1} systematic error in our plate kinematic estimates

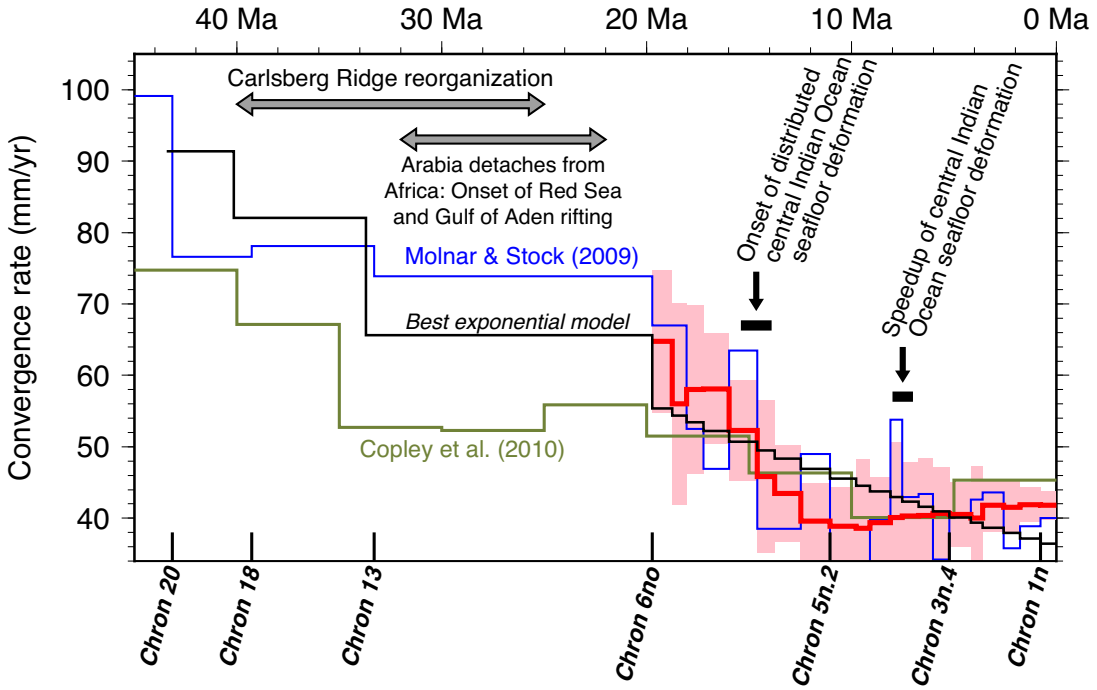

Figure 13. India–Eurasia convergence rates, 45 Ma to present, at 28.0°N, 82.0°E along the Himalayan frontal thrust. Red lines show 19.7-Ma-to-present rates from this study (Table 5). Rates depicted by the blue and olive lines are determined from finite rotations in Table 1 of Molnar & Stock (2009) and Table A1 of Copley *et al.* (2010), respectively. The exponential decay model of Clark (2012) predicts rates (black line) that optimize the fit to the rates estimated with the Molnar & Stock (2009) rotations, but systematically misfit our newly determined India–Eurasia rates.

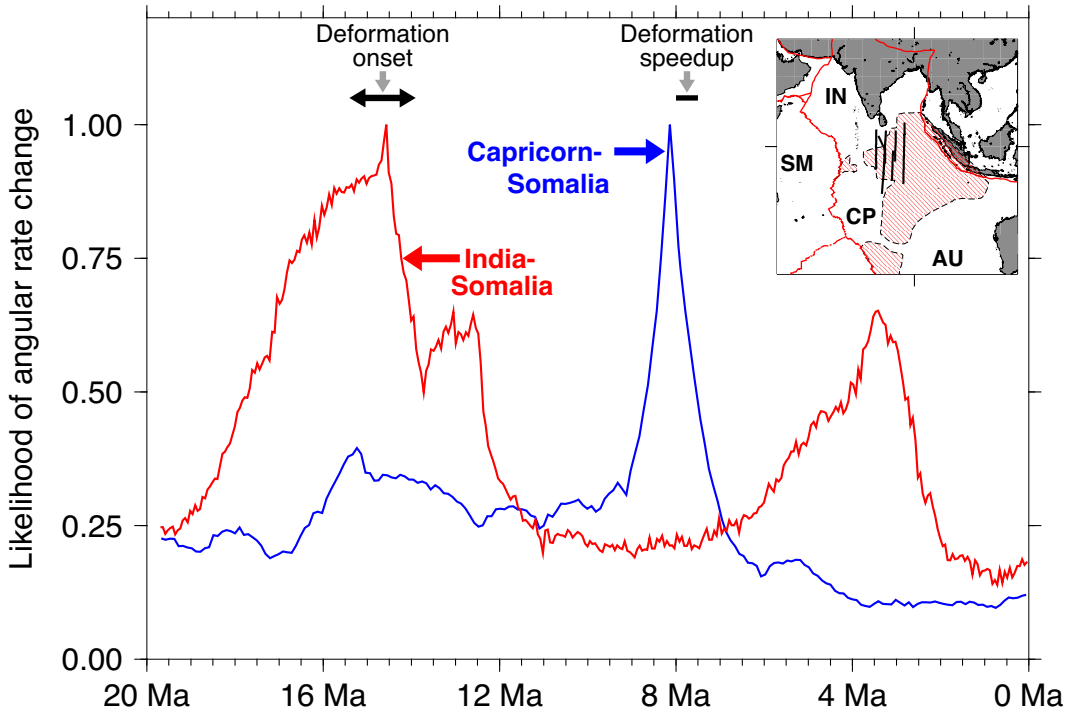

Figure 14. Timing of changes in India–Somalia and Capricorn–Somalia seafloor spreading rates versus ages of central Indian Ocean seafloor deformation determined by Krishna *et al.* (2009) from marine seismic profiles that span most or all of the deforming region indicated by the pink-shaded areas in the map inset. The blue and red curves, respectively, show the normalized probabilities of changes between 0 and 1 during the past 20 Myr in Capricorn–Somalia and India–Somalia angular rotation rates from our REDBACK Bayesian analyses of high-resolution best-fitting rotation sequences from Table 2 of this study and table 3 of DeMets *et al.* (2005). Prior to our REDBACK analysis of the latter rotations, we modified them for an assumed 2-km of outward displacement following methods described by Bull *et al.* (2010) in their supplement. Black lines in the inset map show locations of seismic profiles used by Krishna *et al.* (2009) to estimate the magnitude and timing of the onset and acceleration of distributed seafloor deformation south of India. Plate name abbreviations: AU, Australia; CP, Capricorn; IN, India; SM, Somalia.

to be unlikely given the abundance, redundance, and clarity of the Carlsberg Ridge seafloor spreading data that constrain those estimates (e.g. Fig. 3). A recent acceleration of India–Somalia seafloor spreading rates also seems unlikely to account for the difference, partly because our kinematic analysis indicates that the plate motion has remained steady or nearly steady since at least 10 Ma (Fig. 6a) and partly because a recent speedup of the India Plate's northward motion would also have increased recent convergence rates between India and Eurasia, opposite the slowdown observed via a comparison of our new GPS and plate kinematic estimates (Figs 10 and 12). The differences between our GPS and plate kinematic estimates of India–Somalia and India–Eurasia plate motion thus cannot be resolved easily by invoking a recent slowdown or speedup in India Plate motion or a systematic error in our India Plate angular velocity estimate.

6.4.2 *India–Eurasia*

The new GPS angular velocity for India–Eurasia plate motion (Table 1) predicts instantaneous convergence rates that are 4–5 mm yr^{-1} slower than our plate kinematic estimates (Fig. 12a). It seems unlikely that a recent slowdown in convergence rates between the two plates explains the difference given the plate kinematic evidence for steady or slightly faster convergence rates since 12.47 Ma (Fig. 10a). Some combination of random and/or systematic errors in the geodetic and/or plate kinematic angular velocities must thus be responsible.

The possible sources of error in GPS estimates of India–Eurasia plate motion are numerous. Geodetic angular velocity estimates are influenced by the number, geographic distribution, and time span of the GPS sites that are available to estimate the angular velocity. Angular velocity estimates may also be affected by slow intraplate deformation, drift of geodetic reference frames relative to the geocentre (e.g. Argus 2007), and time-dependent biases in individual GPS site velocities due to transient earthquake afterslip, post-seismic viscoelastic deformation and long-term isostatic and short-term elastic adjustments to the ancient or recent loss of continental ice. We consider some of these below.

Fig. 15(b) shows the wide range of India–Eurasia convergence rates and directions that are predicted at a central location on the plate boundary by nine previously estimated geodetic angular velocities and our own, varying from 33.6 to 43.4 mm yr^{-1} and N10°E–N19°E. The earliest geodetic estimates we considered, those of Paul *et al.* (2001) and Sella *et al.* (2002), differ from each other by 25 per cent and bracket our new plate kinematic estimates (shown by the triangles in Fig. 15b). The more recent Banerjee *et al.* (2008), Argus *et al.* (2010), Altamimi *et al.* (2012), Kreemer *et al.* (2014) and our own angular velocities consistently predict convergence rates of 36.9–37.3 mm yr^{-1}, ≈5 mm yr^{-1} slower than our plate kinematic estimates. The consistency of the recent geodetic estimates may indicate that the 5 mm yr^{-1} discrepancy will not be significantly reduced via future improvements in the number, geographic distribution, or observation time spans of the GPS sites on the India and Eurasia plates.

We investigated whether possible slow tectonic or glacial isostatic deformation within the Eurasia Plate significantly impacts our India–Eurasia GPS angular velocity via a simple test—we separated the 60 Eurasia Plate GPS sites into eastern and western Eurasia Plate subsets on either side of the Ural Mountains at ≈60°E and inverted each of the velocity subsets along with the 29 India Plate GPS site velocities to estimate separate India–East Eurasia and India–West Eurasia angular velocities. The two angular velocities differ by less than 2 angular degrees in location and 3 per cent in their angular rates, indicating that the GPS velocities from sites in eastern and western Eurasia are highly consistent. At a central location on the India–Eurasia plate boundary, the two angular velocities predict India–Eurasia convergence velocities that differ by only 0.6 mm yr^{-1} and 2°, much too small to explain the ≈4-5 mm yr^{-1} difference between the GPS and plate kinematic estimates.

Given the proximity of much of the India Plate to the seismically active Himalayan frontal arc and other earthquake-prone features in the northern and central Indian Ocean, viscoelastic rebound after large earthquakes is a likely though still poorly understood source of systematic bias in GPS velocities for India Plate sites. Whether the combined viscoelastic effects of large historic and recent thrust earthquakes along the Himalayan frontal arc are large enough to explain the aforementioned 4–5 mm yr^{-1} difference between GPS and plate kinematic estimates is unknown, but warrants future investigation. More remote earthquakes also contribute time-dependent biases to velocities measured at India Plate GPS sites. For example, Kreemer *et al.* (2014) and DeMets *et al.* (2017) report changes in the velocities of continuous GPS sites IISC and DGAR after the 26 December 2004 $M_w = 9.3$ Sumatra trench earthquake, both at distances of 2000–3000 km from the 2004 rupture zone. The motions of seven of our 29 India Plate GPS sites were changed measurably by one or both of the 2004 Sumatra trench and 11 April 2012 $M_w = 8.6$ Indian Ocean earthquakes (see for example the GPS coordinate time-series for sites BAN2, IISC and KODI in the Supporting Information). From modeling of the viscoelastic effects of the 2004 earthquake, Shearer & Burgmann (2010) predict cumulative eastward viscoelastic displacements of 100–400 mm by 2064 at sites throughout southern India, and even larger displacements on the island of Sri Lanka. Their modeling implies that sites in southern India will have 1 mm yr^{-1} or larger transient biases in their measured velocities for the foreseeable future.

Random and systematic errors in plate kinematic data and models also contribute to the disagreement noted above, including uncertainties in estimates of magnetic reversal ages, intraplate deformation due to tectonic and thermal effects (Kumar & Gordon 2009), and outward displacement of magnetic reversals due to the finite width of magnetic polarity reversal transition zones (DeMets & Wilson 2008). Evidence that these errors have diminished with time can be found in the progressively better agreement between the velocity predicted by our new GPS-derived India–Eurasia angular velocity and velocities predicted by successive generations of plate kinematic models. The magnitude of the velocity vector difference between our GPS and plate kinematic estimates diminished from 16 to 19 mm yr^{-1} for the early Chase (1972) and Minster & Jordan (1978) plate motion models to 7.9±2 mm yr^{-1} (Fig. 15) for MORVEL (DeMets *et al.* 2010) and 4.6–5.0 mm yr^{-1} for the present study (Fig. 15b). The better agreement with GPS for our new plate kinematic estimates than for the widely used MORVEL plate motion model is principally due to the superior Southwest Indian Ridge reconstructions that we use for this study, which predict present-day motions between the Nubia, Antarctic and Somalia plates that agree better with GPS estimates than does MORVEL (DeMets & Merkouriev 2016; DeMets *et al.* 2017).

Given the abundance of the data that constrain all the global plate circuit rotations that were used in this study, it seems unlikely that a systematic or random error in the angular velocity estimate for any single plate pair in the global circuit is responsible for the entire 5 mm yr^{-1} difference between our new GPS and plate

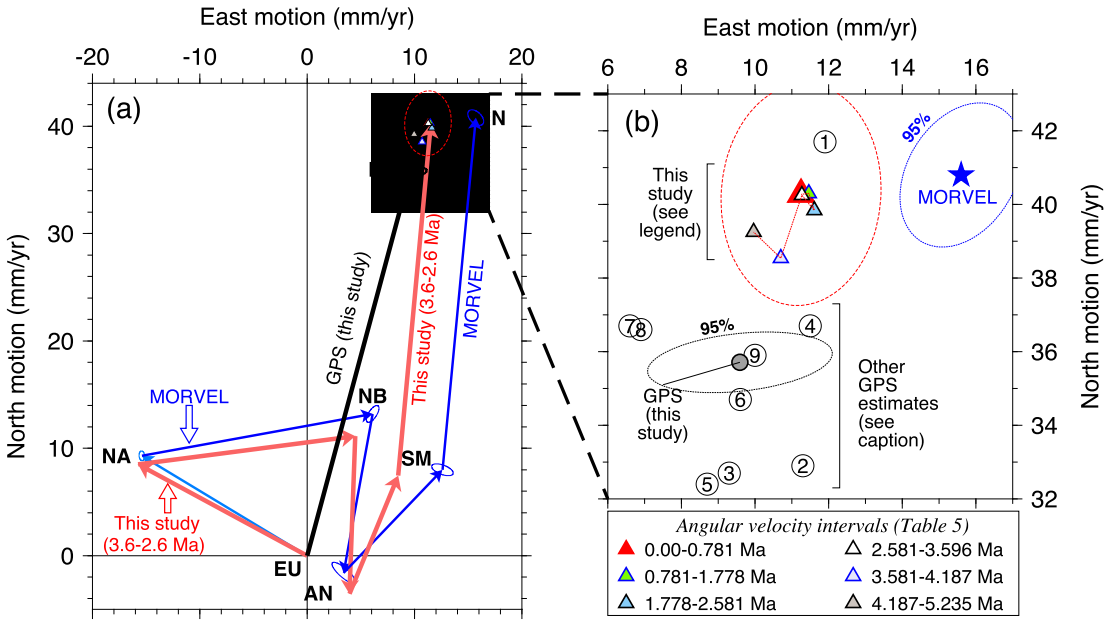

Figure 15. Linear velocities for the Eurasia–North America–Nubia–Antarctic–Somalia–India plate circuit at 28.0°N, 82.0°E along the Himalayan frontal thrust. (a) Velocities for each plate pair estimated with (1) the MORVEL angular velocities (blue vectors), (2) 3.6–2.6-Myr noise-reduced stage rotation from Table 5 and other high-resolution reconstructions cited in the text (red vectors), (3) the India–Eurasia GPS angular velocity in Table 1 (black vector). Triangles show velocity endpoints for other time intervals from Panel B. (b) Expanded view of the India–Eurasia velocities within the shaded rectangle from (a), including nine other geodetic estimates and velocities for five additional intervals between the 5.24 Ma and the present (see legend). For clarity, the velocities are depicted with their endpoints rather than by lines. The triangles demarcate the stage velocities from (a) as determined with the stage angular velocities from Table 5. The numbered circles show geodetic velocities estimated with India–Eurasia angular velocities from 1 - Paul *et al.* (2001), 2 - Sella *et al.* (2002), 3 - Bettinelli *et al.* (2006), 4 - Socquet *et al.* (2006), 5 - Jade *et al.* (2007), 6 - Banerjee *et al.* (2008), 7 - Argus *et al.* (2010), 8 - Altamimi *et al.* (2012), and 9 - Kreemer *et al.* (2014). Plate abbreviations are specified in the legend of Fig. 1. Error ellipses are 2-D, 1σ except where labelled otherwise.

kinematic estimates. Whether the errors and biases that affect the plate kinematic and GPS angular velocity estimates can be reduced enough to diminish to insignificant levels the persistent difference between those estimates remains to be determined.

7 CONCLUSIONS

New estimates of India–Eurasia plate motion at ≈1-Myr intervals since 19.7 Ma are derived by combining finite rotations that reconstruct ≈43 000 magnetic reversal, transform fault, and fracture zone crossings from a global plate circuit that links India to Eurasia via the Somalia, Antarctic, Nubia and North America plates (Fig. 2). These include a new sequence of India–Somalia plate rotations that reconstruct ≈9400 data from the Carlsberg Ridge and northern Central Indian Ridge at 21 times since 19.7 Ma and recently published rotations for the other plate pairs that have not been used previously to estimate India–Eurasia plate motion. Advantages of our new reconstructions relative to previous studies include the following: (1) Motion between Nubia and Somalia, an important source of uncertainty in previous studies, is quantified rigorously via detailed reconstructions of the Southwest Indian Ridge seafloor spreading history. (2) Identical methods and data fitting functions were used to determine all the plate circuit rotations and rotation uncertainties used in this study. (3) Interpolations between rotations, a source of possible artefacts in plate motion determinations, are largely unneeded because the reconstructions for all five plate pairs in the global circuit sample the same 21 magnetic reversals. (4) All the rotation sequences are calibrated to compensate for magnetic reversal outward displacement. (5) Noise-reduced rotation sequences for the global plate circuit are combined and used to describe an India–Eurasia convergence history that is simpler, but that does not significantly degrade the fit to the underlying plate kinematic data.

The principal outcomes of our analysis include:

(1) Evidence that India–Somalia seafloor spreading rates declined 25–30 per cent from 19.7 to 12.5 Ma, but that the pole and rate of angular rotation have changed little or not at all since at least 11.1 Ma or more likely 12.5 Ma.

(2) A relatively simple 20-Ma-to-present India–Eurasia plate motion history, consisting of NNE-directed motion since 19 Ma, a ≈50 per cent decline in India–Eurasia convergence rates from 19.7 to 12.47 Ma or 11.1 Ma, and steady or slightly increasing convergence rates and a stationary pole since 12.47 Ma.

(3) Ten to fifteen per cent differences between our new long-term plate kinematic and instantaneous GPS-derived motion estimates for the India–Somalia and India–Eurasia plate pairs. The differences either imply a rapid change in plate motions during the past few hundred thousand years, which we consider unlikely, or larger-than-expected uncertainties in one or both estimates.

(4) Much closer agreement (40–50 per cent) between the long-term plate kinematic and instantaneous geodetic India–Eurasia motion estimates than was previously the case, a sign of improved accuracy in one or both of the long-term and geodetic estimates.

(5) Inconsistency of the displacements between India and Eurasia calculated with our noise-reduced and best-fitting rotations with the predictions of model that postulates that the rheology of the mantle below Tibet and its steady resistance to the plate convergence have controlled the convergence rate slowdown since at least 50 Ma.

(6) Indirect evidence that the well-timed 8–7.5 Ma acceleration in deformation across the wide oceanic Capricorn–India plate boundary was caused by a change in the forces acting on the Capricorn rather than the India Plate.

ACKNOWLEDGEMENTS

We thank Jean-Phillipe Avouac, Jeff Freymueller and Peter Molnar for reviews that significantly improved the manuscript. This work was supported by grant 06-05-64297 from the Russian Foundation for Basic Research and U.S. National Science Foundation grant OCE-1433323. Sridevi Jade acknowledges the support and encouragement of Head, CSIR-4PI for the GPS programme of CSIR-4PI, and all the scientific and technical personnel involved in operating and maintaining the Indian continuous GPS stations. Continuous GPS data were provided by (1) the Global GNSS Network operated by UNAVCO for NASA Jet Propulsion Laboratory under NSF Cooperative Agreement No. EAR-1261833, (2) the Scripps Orbit and Permanent Array Center and (3) the NOAA CORS archive. Figures were drafted using Generic Mapping Tools software (Wessel & Smith 1991).

REFERENCES

Altamimi, Z., Metivier, L. & Collilieux, X., 2012. ITRF2008 plate motion model, *J. Geophys. Res.,* **117,** B07402, doi: 10.1029/2011JB008930.

Altamimi, Z., Rebischung, P., Metivier, L. & Collilieux, X., 2016. ITRF2014: a new release of the International Terrestrial Reference Frame modeling nolinear staiton motions, *J. geophys. Res.,* **121,** 6109–6131.

Argus, D.F., 2007. Defining the translational velocity of the reference frame of Earth, *Geophys. J. Int.,* **169,** 830–838.

Argus, D.F., Gordon, R.G., Heflin, M.B., Ma, C., Eanes, R., Willis, P., Peltier, W.R. & Owen, S.E., 2010. The angular velocities of the plates and the velocity of Earth's centre from space geodesy, *Geophys. J. Int.,* **180**(3), 913–960.

Banerjee, P., Burgmann, R., Nagarajan, B. & Apel, E., 2008. Intraplate deformation of the Indian subcontinent, *Geophys. Res. Lett.,* **35,** L18301, doi:10.129/2008GL035468.

Bettinelli, P., Avouac, J.-P., Flouzat, M., Jouanne, F., Bollinger, L., Willia, P. & Chitrakar, G., 2006. Plate motion of India and interseismic strain in the Nepal Himalaya from GPS and DORIS measurements, *J. Geod.,* **80,** 567–589.

Bosworth, W., Huchon, P. & McClay, K., 2005. The Red Sea and Gulf of Aden Basins, *J. Afr. Earth Sci.,* **43,** 334–378.

Bull, J.M., DeMets, C., Krishna, K.S., Sanderson, D.J. & Merkouriev, S., 2010. Reconciling plate kinematic and seismic estimates of lithospheric convergence in the central Indian Ocean, *Geology,* **38,** 307–310.

Carbotte, S.M., *et al.*, 2004. New integrated data management system for Ridge2000 and MARGINS research, *EOS, Trans. Am. Geophys. Un.,* **85,** 553–559.

Chang, T., Stock, J. & Molnar, P., 1990. The rotation group in plate tectonics and the representation of uncertainties of plate reconstructions, *Geophys. J. Int.,* **101,** 649–661.

Chase, C.G., 1972. The n-plate problem of plate tectonics, *Geophys. J. R. astr. Soc.,* **29,** 117–122.

Clark, M.K., 2012. Continental collision slowing due to viscous mantle lithosphere rather than topography, *Nature,* **483,** 74–77.

Copley, A., Avouac, J.-P. & Royer, J.-Y., 2010. India-Asia collision and the Cenozoic slowdown of the Indian plate: implications for the forces driving plate motions, *J. geophys. Res.,* **115,** B03410, doi:10.1029/2009JB006634.

DeMets, C., Calais, E. & Merkouriev, S., 2017. Reconciling geologic and geodetic estimates of recent plate motion across the Southwest Indian Ridge, *Geophys. J. Int.,* **208,** 118–133.

DeMets, C., Gordon, R.G. & Argus, D.F., 2010. Geologically current plate motions, *Geophys. J. Int.,* **181,** 1–80.

DeMets, C., Gordon, R.G. & Royer, J.-Y., 2005. Motion between the Indian, Capricorn, and Somalian plates since 20 Ma: Implications for the timing and magnitude of distributed deformation in the equatorial Indian ocean, *Geophys. J. Int.,* **161,** 445–468.

DeMets, C., Iaffaldano, G. & Merkouriev, S., 2015a. High-resolution Neogene and Quaternary estimates of Nubia-Eurasia-North America plate motion, *Geophys. J. Int.,* **203,** 416–427.

DeMets, C. & Merkouriev, S., 2016. High-resolution estimates of Nubia-Somalia plate motion since 20 Ma from reconstructions of the Southwest Indian Ridge, Red Sea and Gulf of Aden, *Geophys. J. Int.,* **207,** 317–332.

DeMets, C., Merkouriev, S. & Sauter, D., 2015b. High-resolution estimates of Southwest Indian Ridge plate motions, 20 Ma to present, *Geophys. J. Int.,* **203,** 1495–1527.

DeMets, C. & Wilson, D.S., 2008. Toward a minimum change model for recent plate motions: Calibrating seafloor spreading rates for outward displacement, *Geophys. J. Int.,* **174,** 825–841.

Dewey, J.F., Cande, S. & Pitman, W.C., 1989. Tectonic evolution of the India/Eurasia collision zone, *Eclogae Geol. Helv.,* **82,** 717–734.

Doubrovine, P.V. & Tarduno, J.A., 2008. A revised kinematic model for the relative motion between Pacific oceanic plates and North America since the Late Cretaceous, *J. geophys. Res.,* **113,** B12101, doi:10.1029/2008JB005585.

Drolia, R.K. & DeMets, C., 2005. Deformation in the diffuse India-Capricorn-Somalia triple junction from a multibeam and magnetic survey of the northern Central Indian ridge, 3°S-10°S, *Geochem., Geophys., Geosys.,* **6,** doi:10.1029/2005GC000950.

Garzione, C., 2008. Surface uplift of Tibet and Cenozoic global cooling, *Geology,* **36,** 1003–1004.

Gibbons, A.D., Zahirovic, S., Muller, R.D., Whittaker, J.M. & Yatheesh, V., 2015. A tectonic model reconciling evidence for the collisions between India, Eurasia and intra-oceanic arcs of the central-eastern Tethys, *Gondw. Res.,* **28,** 451–492.

Gordon, R.G., DeMets, C. & Royer, J.Y., 1998. Evidence for long-term diffuse deformation of the lithosphere of the equatorial Indian Ocean, *Nature,* **395,** 370–374.

Harris, N., 2006. The elevation history of the Tibetan Plateau and its implications for the Asian monsoon, *Palaeogeogr., Palaeoclimatol., Palaeoecol.,* **241,** 4–15.

Hellinger, S.J., 1981. The uncertainties of finite rotations in plate tectonics, *J. geophys. Res.,* **86,** 9312–9318.

Herring, T.A., 2003. GLOBK: global Kalman filter VLBI and GPS analysis program version 10.1, *Internal Memorandum,* Massachusetts Institute of Technology, Cambridge.

Hilgen, F.J., Lourens, L.J. & Van Dam, J.A., 2012. The Neogene Period, in *The Geologic Time Scale 2012,* pp. 947–1002, eds Gradstein, F.M., Ogg, J.G., Schmitz, M. & Ogg, G., Elsevier.

Horner-Johnson, B.C., Gordon, R.G. & Argus, D.F., 2007. Plate kinematic evidence for the existence of a distinct plate between the Nubian and Somalian plates along the Southwest Indian Ridge, *J. geophys. Res.,* **112,** B05418, doi:10292006JB004519.

Iaffaldano, G., Bodin, T. & Sambridge, M., 2012. Reconstructing plate-motion changes in the presence of finite-rotations noise, *Nat. Commun.,* **3,** 1048–1053.

Iaffaldano, G., Bodin, T. & Sambridge, M., 2013. Slow-downs and speed-ups of India–Eurasia convergence since ≈20 Ma: data-noise, uncertainties and dynamic implications, *Earth planet. Sci. Lett.,* **367,** 146–156.

Iaffaldano, G., Davies, D.R. & DeMets, C., 2018. Indian Ocean floor deformation induced by the Reunion plume rather than the Tibetan Plateau, *Nat. Geosci.,* **11,** 362–366.

Iaffaldano, G., Hawkins, R., Bodin, T. & Sambridge, M., 2014. REDBACK: Open-source software for efficient noise-reduction in plate kinematic reconstructions, *Geochem. Geophys. Geosys.,* **15,** 1663–1670.

Jade, S. *et al.*, 2007. Estimates of interseismic deformation in Northeast India from GPS measurements, *Earth planet. Sci. Lett.,* **263,** 221–234.

Jade, S., Shrungeshwara, T.S., Kumar, K., Choudhury, P., Dumka, R.K. & Bhu, H., 2017. India plate angular velocity and contemporary deformation rates from continuous GPS measurements from 1996 to 2015, *Scient. Rep.,* **7,** 11439.

Kirkwood, B.H., Royer, J.-Y., Chang, T.C. & Gordon, R.G., 1999. Statistical tools for estimating and combining finite rotations and their uncertainties, *Geophys. J. Int.,* **137,** 408–428.

Klootwijk, C.T., Gee, J.S., Peirce, J.W. & Smith, G.M., 1992. An early India-Asia contact: paleomagnetic constraints from Ninetyeast ridge, ODP Leg 121, *Geology,* **20,** 395–398.

Kreemer, C., Blewitt, G. & Klein, E.C., 2014. A geodetic plate motion and Global Strain Rate Model, *Geochem. Geophys. Geosys.,* **15,** 3849–3889.

Krishna, K.S., Bull, J.M. & Scrutton, R.A., 2009. Early (pre 8 Ma) fault activity and temporal strain accumulation in the central Indian Ocean, *Geology,* **37,** 227–230.

Kumar, R.V. & Gordon, R.G., 2009. Horizontal thermal contraction of oceanic lithosphere: the ultimate limit to the rigid plate approximation, *J. geophys. Res.,* **114,** B01403, doi:10.1029/2007JB005473.

Lemaux, J., Gordon, R.G. & Royer, J.-Y., 2002. Location of the Nubia-Somalia boundary along the Southwest Indian Ridge, *Geology,* **30,** 339–342.

Mercuriev, S., Patriat, P. & Sochevanova, N., 1995. Evolution de la dorsale de Carlberg: evidence pour une phase d'expansion tres lente entre 40 et 25 Ma (A18 a A7), *Oceanol. Acta,* **19,** 1–13.

Merkouriev, S. & DeMets, C., 2006. Constraints on Indian plate motion since 20 Ma from dense Russian magnetic data: implications for Indian plate dynamics, *Geochem. Geophys. Geosyst.,* **7,** Q02002, doi:10.1029/2005GC001079.

Merkouriev, S. & DeMets, C., 2014a. High-resolution estimates of Nubia-North America plate motion: 20 Ma to present, *Geophys. J. Int.,* **196,** 1281–1298.

Merkouriev, S. & DeMets, C., 2014b. High-resolution Quaternary and Neogene reconstructions of Eurasia-North America plate motion, *Geophys. J. Int.,* **198,** 366–384.

Minster, J.B. & Jordan, T.H., 1978. Present-day plate motions, *J. geophys. Res.,* **83,** 5331–5354.

Molnar, P., England, P. & Martinod, J., 1993. Mantle dynamics, uplift of the Tibetan Plateau, and the Indian monsoon, *Rev. Geophys.,* **31,** 357–396.

Molnar, P. & Stock, J.M., 2009. Slowing of India's convergence with Eurasia since 20 Ma and its implications for Tibetan mantle dynamics, *Tectonics,* **28,** TC3001, doi:10.1029/2008TC002271.

Molnar, P. & Tapponnier, P., 1975. Cenozoic tectonics of Asia: effects of a continental collision, *Science,* **189,** 419–426.

Ogg, J.G., 2012. Geomagnetic polarity time scale, in *The Geologic Time Scale 2012,* pp. 85–113, eds Gradstein, F.M., Ogg, J.G., Schmitz, M. & Ogg, G., Elsevier, doi:10.1016/B978-0-444-59425-9.00005-6.

Patriat, P. & Achache, J., 1984. India–Eurasia collision chronology has implications for crustal shortening and driving mechanism of plates, *Nature,* **311,** 615–621.

Patriat, P. & Segoufin, J., 1988. Reconstruction of the central Indian Ocean, *Tectonophysics,* **155,** 211–234.

Paul, J., *et al.*, 2001. The motion and active deformation of India, *Geophys. Res. Lett.,* **28,** 647–651.

Raymo, M.E. & Ruddiman, W.F., 1992. Tectonic forcing of late Cenozoic climate, *Nature,* **359,** 117–122.

Royer, J.-Y. & Chang, T., 1991. Evidence for relative motions between the Indian and Australian plates during the last 20 Myr from plate tectonic reconstructions: Implications for the deformation of the Indo-Australian plate, *J. geophys. Res.,* **96,** 11 779–11 802.

Royer, J.-Y., Gordon, R.G. & Horner-Johnson, B.C., 2006. Motion of Nubia relative to Antarctica since 11 Ma: Implications for Nubia-Somalia, Pacific-North America, and India–Eurasia motion, *Geology,* **34,** 501–504.

Saria, E., Calais, E., Stamps, D.S., Delvaux, D. & Hartnady, C.J.H., 2014. Present-day kinematics of the East African Rift, *J. geophys. Res.,* **119,** 3584–3600.

Sella, G.F., Dixon, T.H. & Mao, A., 2002. REVEL: a model for recent plate velocities from space geodesy, *J. geophys. Res.,* **107**(B4), doi:10.1029/2000JB000033.

Shaw, P.R. & Cande, S.C., 1990. High-resolution inversion for South Atlantic plate kinematics using joint altimeter and magnetic anomaly data, *J. geophys. Res.,* **95,** 2625–2644.

Shearer, P. & Burgmann, R., 2010. Lessons learned from the 2004 Sumatra-Andaman megathrust rupture, *Annu. Rev. Earth planet. Sci.,* **38,** 103–132.

Socquet, A., Vigny, C., Chamot-Rooke, N., Simons, W., Rangin, C. & Ambrosius, B., 2006. India and Sunda plates motion and deformation along their boundary in Myanmar determined by GPS, *J. geophys. Res.,* **111,** B05406.

Wessel, P. & Smith, W.H.F., 1991. Free software helps map and display data, *EOS, Trans. Am. Geophys. Un.,* **72,** 441–446.

White, L. & Lister, G., 2012. The collision of India with Asia, *J. Geodyn.,* **56-57,** 7–17.

Wolfenden, E., Ebinger, C., Yirgu, G., Renne, P.R. & Kelley, S.P., 2005. Evolution of a volcanic rifted margin: Southern Red Sea, Ethiopia, *Bull. Geol. Soc. Am.,* **117,** 846–864.

Zumberge, J.F., Heflin, M.B., Jefferson, D.C., Watkins, M.M. & Webb, F.H., 1997. Precise point positioning for the efficient and robust analysis of GPS data from large networks, *J. geophys. Res.,* **102,** 5005–5017.

DeMets, C. & Wilson, D.S., 2008. Toward a minimum change model for recent plate motions: Calibrating seafloor spreading rates for outward displacement, *Geophys. J. Int.,* **174,** 825–841.

SUPPORTING INFORMATION

Supplementary data are available at *GJI* online.

ENU_DailyGPS_AllSites.zip
Supplement_GJI19-0564.pdf

Please note: Oxford University Press is not responsible for the content or functionality of any supporting materials supplied by the authors. Any queries (other than missing material) should be directed to the corresponding author for the paper.